The sensitivity of Southern Ocean atmospheric dimethyl sulfide to modelled sources and emissions

Yusuf A. Bhatti[1], Laura E. Revell[1], Alex J. Schuddeboom[1,*], Adrian J. McDonald[1,2], Alex T. Archibald[3,4], Jonny Williams[5], Abhijith U. Venugopal[1], Catherine Hardacre[6,#], and Erik Behrens[5]

[1]School of Physical and Chemical Sciences, University of Canterbury, Christchurch, New Zealand
[2]Gateway Antarctica, University of Canterbury, Christchurch, New Zealand
[3]National Centre for Atmospheric Science, Cambridge, United Kingdom
[4]Yusuf Hamied Department of Chemistry, University of Cambridge, Cambridge, United Kingdom
[5]National Institute of Water and Atmospheric Research (NIWA), Wellington, New Zealand
[6]Met Office, Exeter, EX1 3PB, United Kingdom
[*]Now at National Institute of Water and Atmospheric Research (NIWA), Christchurch, New Zealand
[#]Now at School of Physical and Chemical Sciences, University of Canterbury, Christchurch, New Zealand

Correspondence: Yusuf Bhatti (yusuf.bhatti@pg.canterbury.ac.nz)

Abstract. The biogeochemical behavior of the Southern Ocean is complex and dynamic and driven by physical, chemical, and biological processes. Such processes leads to the formation of dimethyl sulfide (DMS), which is produced by marine biogenic activity and is the dominant source of sulfate aerosol over the Southern Ocean. However, DMS production is poorly constrained in Earth system models. Using an atmosphere-only nudged to observations configuration of the United Kingdom Earth System Model (UKESM1-AMIP), we performed eight 10-year simulations for the recent past (2009–2018). We tested four seawater DMS data sets and three DMS sea-to-air transfer velocity parameterizations. All data sets and parameterizations are commonly used by present-day Earth system models, with the exception of one data set that we developed from satellite chlorophyll-a data. We evaluate simulated oceanic DMS, sea-to-air transfer of DMS, and atmospheric DMS during austral summer. In simulations with different seawater DMS data sets but the same sea-to-air flux parameterization, Southern Ocean summertime DMS varies by 112% (3.3 to 6.9 TgS Yr^{-1}). This is approximately twice as much as the simulations using the same seawater DMS data set but differing sea-to-air flux parameterizations, in which DMS varies by 50-60% (2.9 to 4.7 TgS Yr^{-1}). The choice of oceanic DMS source has a larger influence on atmospheric DMS than the choice of DMS emission. Simulations testing different sea-to-air transfer velocity parameterizations show that simulating a linear dependence of DMS gas transfer velocity as a function of wind speed results in a more accurate representation of atmospheric DMS distributions than using quadratic relationships. Simulations using seawater DMS derived from satellite chlorophyll-a data show realistic spatiotemporal variability in DMS and when combined with a recently developed transfer velocity parameterization for DMS, the model shows good agreement with atmospheric DMS observations. As a precursor for natural sulfate aerosol and cloud condensation nuclei, DMS plays an important role in the radiative balance over the Southern Ocean. This work highlights that the seawater DMS data sets and sea-to-air transfer velocity parameterizations for DMS commonly used in climate models are poorly constrained for the Southern Ocean region. We recommend that models use a DMS sea-to-air parameterization that was developed specifically for DMS, and for oceanic DMS datasets to incorporate spatial variability based on observed marine

biogenic activity. Such improvements will provide a more accurate process-based representation of oceanic and atmospheric DMS, and therefore sulfate aerosol, in the Southern Ocean region.

1 Introduction

The representation of aerosols over the Southern Ocean is a large source of uncertainty in climate models due to the lack of observational data and large seasonal variability (Revell et al., 2019). Poor representation of aerosols contributes to the large biases in future climate projections over the Southern Ocean (Myhre et al., 2014). Sea spray and dimethyl sulfide (DMS; CH_3SCH_3) are fundamental sources for aerosol formation over this region (Revell et al., 2021; Bhatti et al., 2022). The dominant source of sulfate over the marine atmosphere is the biogenic marine aerosol precursor DMS, controlled by marine biota (Keller et al., 1989; Bates et al., 1987; Kiene and Bates, 1990; Curson et al., 2011). Revell et al. (2019) found sulfate aerosol production from DMS was responsible for around 60% of the austral summer aerosol optical depth over the Southern Ocean. Atmospheric DMS therefore has the potential to greatly influence cloud condensation nuclei during austral summer (Kloster et al., 2006; Revell et al., 2019; Korhonen et al., 2008; Pandis et al., 1994).

The Southern Ocean contains extremely high phytoplankton and marine biota productivity during austral summer (DJF, December–February) (Deppeler and Davidson, 2017). Marine biogenic activity plays a key role in chlorophyll-a (chl-a) production and is considered to be a key driver of oceanic DMS production (e.g. Uhlig et al., 2019; Townsend and Keller, 1996; Anderson et al., 2001; Deppeler and Davidson, 2017). Earth System Models (ESMs) represent the process of oceanic DMS formation through multiple approaches that are dependent on chl-a, nutrients, light, mixed-layer depth, zooplankton, and dimethylsulfoniopropionate concentration (Bock et al., 2021). The UKESM1 and MIROC-ES2L models use a diagnostic approach to represent chl-a (Sellar et al., 2019; Anderson et al., 2001; Hajima et al., 2020). The CNRM-ESM2-1 and NorESM2-LM models use a prognostic approach, closely related to zooplankton and dimethylsulfoniopropionate abundance, which are both precursors of oceanic DMS (Seland et al., 2020; Séférian et al., 2019). Bock et al. (2021) evaluated oceanic DMS in CMIP6 models and found that all models are biased in comparison with observational climatologies of DMS in the Southern Ocean region.

Atmosphere-only global climate models use climatologies to prescribe the global concentration of oceanic DMS. Lana et al. (2011) and Kettle et al. (1999) constructed observational climatologies of oceanic DMS which are used by such models. However, there is a limited amount of data available within the Southern Ocean, which can lead to errors in the representation of oceanic DMS (e.g. Bock et al., 2021; Mulcahy et al., 2020). A limitation of representing oceanic DMS as a static climatology is that it does not account for the large temporal variations in DMS concentrations observed. For instance, El Niño Southern Oscillation (ENSO) events, wildfires, and volcanic eruptions all significantly influence oceanic DMS within the Southern Ocean (e.g. Yoder and Kennelly, 2003; Tang et al., 2021; Wang et al., 2022; Browning et al., 2015; Longman et al., 2022). Calculating oceanic DMS online using a biological proxy would resolve these perturbing events to some degree (Galí et al., 2018).

The flux of DMS from the ocean to the atmosphere depends on the gas transfer velocity, which in turn depends on the surface wind speed (e.g. Fairall et al., 2011). Many DMS flux parameterizations have been developed, but most use transfer velocities measured for gases other than DMS (Wanninkhof, 1992, 2014; Nightingale et al., 2000; Liss and Merlivat, 1986). Some studies, including Blomquist et al. (2017) and Yang et al. (2011), used DMS measurements to derive a relationship between wind speed and DMS. Depending on the solubility of the gas measured, gas transfer velocities typically have a linear or quadratic dependence on wind speed. Linear relationships best represent gases with intermediate solubilities, such as DMS (e.g. Blomquist et al., 2017; Goddijn-Murphy et al., 2016; Bell et al., 2015; Yang et al., 2011; Huebert et al., 2010), while quadratic equations are better suited for highly soluble gases like CO_2 (Wanninkhof, 2014; Nightingale et al., 2000; Wanninkhof, 1992).

Uncertainty in DMS emissions remains high, particularly in the Southern Ocean region where wind speeds are high and observational data sparse (e.g. Elliott, 2009; Smith et al., 2018; Zhang et al., 2020). ESMs use a variety of transfer velocities to represent DMS emissions (Bock et al., 2021). UKESM1 uses the Liss and Merlivat (1986) parameterization even though it was constructed for gases other than DMS.

Here we examine whether incorporating realistic oceanic DMS variability, based on remotely-sensed chl-a observations improves the simulation of atmospheric DMS. Using a nudged configuration of the atmosphere-only United Kingdom Earth System Model (UKESM1-AMIP), we use three established oceanic DMS datasets and three transfer velocity parameterizations. We also test a 10-year monthly time series in which seawater DMS is calculated offline from MODIS-aqua satellite chl-a data using the Anderson et al. (2001) oceanic DMS parameterization which is used by UKESM1 (Sellar et al., 2019). We evaluate sea-to-air fluxes of DMS and oceanic and atmospheric DMS concentrations relative to station and ship-based observations. The observational data sets are described in Section 2.4, the model configuration is described in Section 2.1, and details of the oceanic DMS data sets and sea-to-air transfer velocity parameterizations tested are in Sections 2.2 and 2.3, respectively. Results follow in Section 3.

2 Methods

2.1 Model Configuration and Evaluation

Simulations were performed using the atmosphere-only configuration of the coupled UK Earth System Model (UKESM1; Yool et al., 2020; Sellar et al., 2019; Mulcahy et al., 2020). By default, atmospheric DMS is produced via the Lana et al. (2011) oceanic DMS data set and Liss and Merlivat (1986) sea-to-air transfer velocity parameterization. Atmospheric DMS then oxidises to form sulfate aerosols. In UKESM1, aerosol growth, chemistry and removal are handled by the GLOMAP-mode scheme (Mulcahy et al., 2020).

Wind and temperatures are nudged to 6-hourly ERA-5 reanalysis data (Hersbach et al., 2020). The full description of the nudging configuration is outlined in Telford et al. (2008). Nudging ensures that wind speeds, which are pivotal to the formation of atmospheric DMS, are accurately represented (Pithan et al., 2022; Kuma et al., 2020) and allows like-for-like comparisons against observations. Sea surface temperature and sea ice data from The Hadley Centre Global Sea Ice and Sea Surface Tem-

Table 1. Oceanic DMS data sets used in the model simulations.

Oceanic DMS dataset	Source	Citation	Year of Data
Lana	Oceanic DMS observations	Lana et al. (2011)	1972 - 2009
Hulswar	Oceanic DMS observations	Hulswar et al. (2022)	1972 - 2021
MEDUSA	UKESM1 CMIP6 simulations	Anderson et al. (2001); Sellar et al. (2019)	1979 - 2014
MODIS-DMS	MODIS-aqua chlorophyll-a via Anderson et al. (2001)	N/A (produced for this study)	2009 - 2018

perature were used (HadISST; Titchner and Rayner, 2014). Simulations are 10 years long, spanning from 2009 to 2018. This period was chosen to coincide with the availability of recent DMS observations (Section 2.4).

Atmospheric DMS concentrations are analyzed at the lowest model level, at 20 m during DJF, which is the most productive season for DMS (Deppeler and Davidson, 2017; Jarníková and Tortell, 2016). Hourly output was saved to compare with observations where applicable (for example, voyages provide observations at hourly temporal frequency). To evaluate variability, we use the coefficient of variation (CoV). A higher CoV suggests that the variability or dispersion of the data is relatively large compared to its mean. Where uncertainty is reported, one standard deviation calculated over the relevant domain and time period is stated.

2.2 Oceanic DMS

We input four oceanic DMS data sets into the model: three climatologies and one 10-year time series. Observational-based climatologies are from Lana et al. (2011) (hereafter 'Lana') and Hulswar et al. (2022) ('Hulswar'). The 'MEDUSA' climatology (1979-2014) originates from the UKESM1 CMIP6 (Yool et al., 2021; Sellar et al., 2019; Tang et al., 2019). Table 1 outlines the oceanic DMS datasets used. Ocean biogeochemistry is simulated in the UKESM1 via MEDUSA2.0 (the Model of Ecosystem Dynamics, nutrient Utilization, Sequestration, and Acidification; Yool et al., 2020, 2013). The time series was calculated offline using a combination of satellite data and the UKESM1 approach to calculating seawater DMS, as described below.

In UKESM1, oceanic DMS concentrations are calculated using a diagnostic method from Anderson et al. (2001), using surface daily shortwave radiation (J), dissolved inorganic nitrogen (Q), and chl-a (C):

$$Oceanic\ DMS = a,\ for\ log(CJQ) \leq s \tag{1}$$

$$Oceanic\ DMS = b[log(CJQ) - s] + 1,\ for\ log(CJQ) > s \tag{2}$$

The parameter values are a=1, b=8, and s=1.56, as described by Sellar et al. (2019). Q, chl-a, and J are averaged from CMIP6 for the MEDUSA climatology. The Anderson et al. (2001) parameterization produces positive biases in DMS over the Southern Ocean within MEDUSA (Bock et al., 2021) due to the set minimum oceanic concentration of 1, which leads to

large average DMS concentrations (Yool et al., 2021; Bock et al., 2021). Recent research suggests that chl-a may not be an appropriate proxy for oceanic DMS (Uhlig et al., 2019; Bell et al., 2021), and future work will explore alternative methods for calculating oceanic DMS within UKESM1. Nonetheless, chl-a is widely used by CMIP6-era models to calculate oceanic DMS, and we explore here whether using an observationally derived chl-a concentration field leads to changes in the spatial and temporal variability of atmospheric DMS. Monthly-mean chl-a concentrations from the Moderate Resolution Imaging Spectroradiometer (MODIS)-aqua satellite instrument were used to construct a time series of oceanic DMS between 2009–2018 (Table 1; Hu et al., 2019; O'Reilly and Werdell, 2019). This time series, which we term the 'MODIS-DMS' data set, is calculated offline using the same diagnostic parameterization as Equations 1 and 2. The J and Q used to calculate MODIS-DMS remain the same as MEDUSA. Through this, we capture spatial and interannual chl-a variability, indicating biological productivity. Bi-linear interpolation is used to fill in small gaps (around 1% for monthly averages) of spatial chl-a data. Oceanic DMS concentrations are masked where they coincide within the sea-ice zone from HadISST.

In general, the MODIS-aqua Ocean Color chl-a retrieval underestimates Southern Ocean chlorophyll concentrations (Zeng et al., 2016; Haëntjens et al., 2017; Jena, 2017; Gregg and Casey, 2007; Johnson et al., 2013). Simulated oceanic DMS may therefore be systematically underestimated. Nonetheless, the high spatial and temporal availability of chl-a observations during summertime makes it useful to explore spatiotemporal variability in atmospheric DMS.

2.3 DMS Sea-to-Air Flux

Three DMS transfer velocities are tested (Figure 1, Table 2). Two are linear equations from Liss and Merlivat (1986) (hereafter 'LM86') and Blomquist et al. (2017) (hereafter 'B17'). LM86 is the default parameterization within UKESM1 (Sellar et al., 2019) and was evaluated in combination with all oceanic DMS data sets. The quadratic formula from Wanninkhof (2014) (hereafter 'W14') is also tested. Using these different parameterizations provides an appropriate estimate for the spread of DMS emissions due to the upper and lower limits of DMS transfer velocity tested from in-situ DMS measurements (e.g. Goddijn-Murphy et al., 2016; Blomquist et al., 2017). Table 2 summarizes the sensitivity simulation names performed. Simulations are named with the oceanic DMS concentration used, subscripted with the sea-to-air transfer velocity used. For example, Lana$_{LM86}$ means that the simulation used the Lana et al. (2011) climatology as its oceanic DMS source, and the DMS transfer velocity parameterization of Liss and Merlivat (1986).

The Schmidt number for DMS is used to calculate the DMS emission. The Schmidt number represents the viscosity/diffusion properties of a gas, varying with respect to sea surface temperature (T in °C). We update the Schmidt number of DMS (Sc_{DMS}) used in the UKESM1 from the formulation used in Saltzman et al. (1993) to Wanninkhof (2014), as shown in Equation 3:

$$Sc_{DMS} = 2855.7 + (-177.63 + (6.0438 + (-0.11645 + 0.00094743 \cdot T) \cdot T) \cdot T) \cdot T \quad (3)$$

Where T is derived from HadISST (Titchner and Rayner, 2014). U_{10} (m s^{-1}) represents near-surface (10 m) wind speed and K_w (cm h^{-1}) represents the transfer velocity of DMS. Equation 4 represents the LM86 transfer velocity of DMS:

Table 2. Simulations used in this study, named with the oceanic DMS concentration used, subscripted with the sea-to-air transfer velocity used.

Simulation name	Oceanic DMS source	DMS transfer velocity parameterization
Lana$_{LM86}$	Lana et al. (2011)	Liss and Merlivat (1986)
Lana$_{B17}$	Lana et al. (2011)	Blomquist et al. (2017)
Lana$_{W14}$	Lana et al. (2011)	Wanninkhof (2014)
Hulswar$_{LM86}$	Hulswar et al. (2022)	Liss and Merlivat (1986)
MEDUSA$_{LM86}$	Anderson et al. (2001); Sellar et al. (2019)	Liss and Merlivat (1986)
MODIS$_{LM86}$	N/A (produced for this study)	Liss and Merlivat (1986)
MODIS$_{B17}$	N/A (produced for this study)	Blomquist et al. (2017)
MODIS$_{W14}$	N/A (produced for this study)	Wanninkhof (2014)
MODIS$_{B17}$CLIM	N/A (climatology produced for this study)	Blomquist et al. (2017)

for $u_{10} \leq 3.6$:

$$K_w = 0.17 \left(\frac{600}{Sc_{DMS}} \right)^{\frac{2}{3}} u_{10},$$

for $3.6 \leq u_{10} < 13$:

$$K_w = 2.85 \left(\frac{600}{Sc_{DMS}} \right)^{\frac{1}{2}} (u_{10} - 3.6) + 0.612 \left(\frac{600}{Sc_{DMS}} \right)^{\frac{2}{3}},$$

for $u_{10} > 13$:

$$K_w = 5.9(u_{10} - 13) \left(\frac{600}{Sc_{DMS}} \right)^{\frac{1}{2}} + 26.79(u_{10} - 3.6) \left(\frac{600}{Sc_{DMS}} \right)^{\frac{1}{2}} + 0.612 \left(\frac{600}{Sc_{DMS}} \right)^{\frac{2}{3}} \quad (4)$$

W14 uses a quadratic formula (equation 5) for sea-to-air transfer. W14 is also used to calculate DMS emissions amongst CMIP6 models (e.g. Tjiputra et al., 2020).

$$K_w = 0.251 \cdot u_{10}^2 \left(\frac{660}{Sc_{DMS}} \right)^{\frac{1}{2}} \quad (5)$$

145 B17 is the only parameterization tested in this study for which the transfer velocity is based on real-world observation of DMS (Equation 6). B17 is a superlinear parameterization, however, for simplicity and the wind speeds used in this study, we label B17 as a linear parameterization.

$$K_w = 0.7432 \cdot u_{10}^{1.33} \left(\frac{660}{Sc_{DMS}} \right)^{\frac{1}{2}} \quad (6)$$

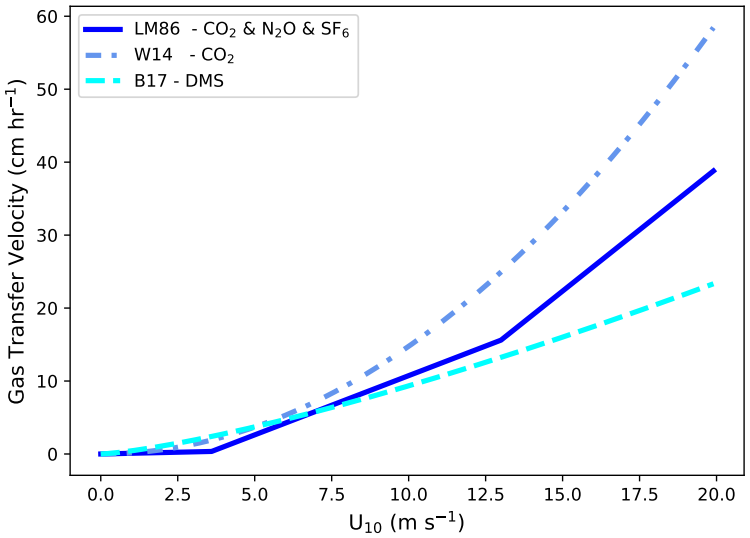

Figure 1. DMS transfer velocities tested in this study. LM86 = Liss and Merlivat (1986); W14 = Wanninkhof (2014); B17 = Blomquist et al. (2017). The gases labelled in the legend are the measurements taken to identify the gas exchange relationship.

To assess the inter-annual variability of DMS emissions and atmospheric DMS concentrations, we performed an additional 10-year simulation, MODIS$_{B17}$CLIM. While MODIS$_{B17}$ used a 10-year time series of oceanic DMS derived from MODIS chlorophyll-a data, MODIS$_{B17}$CLIM used a climatology calculated from monthly-mean data for the 10-year MODIS$_{B17}$ time series.

2.4 Observational Datasets

2.4.1 DMS Datasets

Two Southern Ocean voyages are used to evaluate our simulations: the SOAP campaign (Surface Ocean Aerosol Production; Bell et al., 2015; Law et al., 2017) and RV Tangaroa voyage (TAN1802; Kremser et al., 2021). The SOAP voyage measured oceanic and atmospheric DMS from Feb-March 2012 near the Chatham Rise (within 42–47 °S, 172–180 °E) off the east coast of New Zealand (Bell et al., 2015; Smith et al., 2018). The TAN1802 voyage measured oceanic DMS along the Southern Ocean during Feb-March 2018 between 40 °S to 70 °S, 180 °E (Kremser et al., 2021). We also extend the simulations to cover the ANDREXII voyage between Feb - April 2019 for atmospheric DMS concentrations as this voyage mostly measured during autumn (Wohl et al., 2020). ANDREXII traveled longitudinally around 60 °S. Although outside our simulation range, we also consider SOIREE for atmospheric DMS analysis from Feb 1999 (Boyd and Law, 2001) between 42 - 63 °S, 139–172 °E.

We used oceanic DMS measurements for TAN1802 Kremser et al. (2021), SOAP (Bell et al., 2015), and ERA-5 surface wind speeds (Hersbach et al., 2020) to calculate hourly DMS emissions. The Wanninkhof (2014) DMS Schmidt number is calculated using the same parameters used within the simulations, for consistency with comparisons to simulated fluxes. The HadISST and ERA-5 wind speed data were obtained for the same time and location as the two voyages (within the nearest neighbor grid cell). We applied three different sea-to-air flux parameterizations (LM86, B17, and W14) to both SOAP and TAN1802 voyage paths (See section 3.2).

We compare our simulations to the voyage dataset using the hourly model output and identify the nearest neighbor grid cell to the ship location. Analysis of oceanic DMS data used in the models is also synchronized to TAN1802 and SOAP voyages, using the same timescales for comparing the voyages with model data.

We also validate the model using atmospheric DMS concentrations measured at two stations: Cape Grim (1989 to 1996; 41 °S and 145 °E) and King Sejong Station (2018 to 2020; 62 °S, 58 °W). King Sejong is located on the Antarctic Peninsula, where sea ice melt occurs during our study period, which can profoundly increase DMS emissions, as previously found by Berresheim et al. (1998); Read et al. (2008).

2.4.2 Cloud and Aerosol Observations

MODIS-aqua aerosol optical depth (AOD) measurements at 550 nm (Platnick et al., 2017) are compared with each daily-mean model output. Daily-averaged observations from Grosvenor et al. (2018) and Bennartz and Rausch (2017) were used to compare the cloud droplet number concentration (CDNC) with our daily-averaged simulations. Finally, to evaluate cloud condensation nuclei (CCN), we used Choudhury and Tesche (2023) at 818 m, in comparison with simulated CCN at 800 m. The description and evaluation of using MODIS-observed AOD compared with a related configuration of UKESM1-AMIP is discussed in more detail in Revell et al. (2019) and Mulcahy et al. (2020). We calculate an austral summertime climatology for these observational datasets, which we use over the Southern Ocean.

3 Results and Discussion

3.1 Oceanic DMS

Figure 2a-d shows the spatial distribution of each oceanic DMS dataset. Each distribution has key defining characteristics, although Hulswar (Figure 2d) is an update to Lana (Figure 2c). The distinction between MODIS-DMS and MEDUSA oceanic DMS calculations is chl-a, which results in distinctly different distributions, as shown in Figure 2e. Observational-based climatologies, like Lana or Hulswar, do not align with the chl-a distribution in the Southern Ocean, particularly along the Antarctic Circumpolar Current, concentrating oceanic DMS in specific regions based only on observations of oceanic DMS (Lana et al., 2011; Hulswar et al., 2022). The mean difference between the lowest (MODIS-DMS) and highest (MEDUSA) mean of all the oceanic DMS datasets used is 107%.

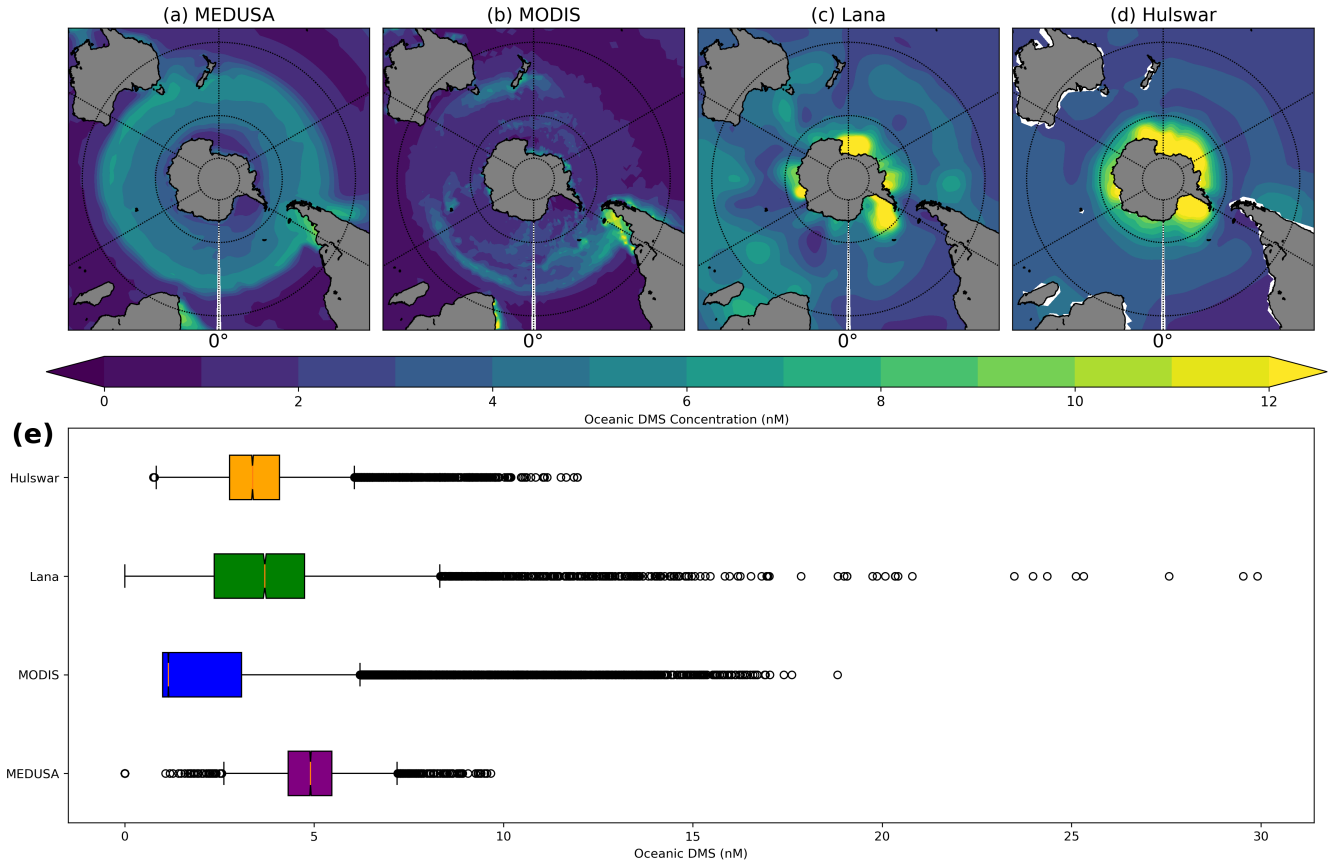

Figure 2. Summertime (DJF) Oceanic DMS in the Southern Ocean (40 - 60 °S). The spatial distribution (a-d) shows the (a) UKESM1 climatology from MEDUSA, (b) the climatology from MODIS-DMS, and observational-based climatologies of (c) Lana and (d) Hulswar. (e) The box plot shows the distribution of each oceanic DMS dataset used, where MODIS-DMS contains all 10 years of data, while the climatologies contain 12 months.

MEDUSA produces the most homogeneous oceanic DMS distribution in the summertime Southern Ocean, with the highest mean and smallest standard deviation (4.88±0.87 nM). It also has the lowest CoV of ±17% indicating a small spread of variance. Chl-a in MEDUSA shows a positive bias against summer observations in the Southern Ocean (Yool et al., 2013, 2021). In contrast, MODIS-DMS has low oceanic DMS concentrations in open ocean regions, and high concentrations in biologically productive regions (near the subtropical front), such as the Chatham Rise and coastal South America (Behrens and Bostock, 2023). MODIS-DMS has the largest spatial variability in oceanic DMS overall (CoV 67%). The mean oceanic DMS in MODIS-DMS is 2.36±1.57 nM, which is outside the range of MEDUSA, highlighting the sensitivity of the Anderson et al. (2001) parameterization to chl-a concentrations.

In the MODIS-DMS simulation, oceanic DMS concentrations vary each summer across the Southern Ocean over a 10-year climatology (See Figure **??**a in the appendix). The most significant interannual variability occurs around New Zealand and

South America's East Coast, likely from phytoplankton blooms influenced by ENSO (e.g. Santoso et al., 2017; Thompson et al., 2015; Yoder and Kennelly, 2003) (Figure 2a). The Lana and Hulswar simulations have similar means (3.87 nM and 3.51 nM, respectively) but differ in their distribution (Figure 2e). Oceanic DMS maximises at 30 nM in Lana, and at 14 nM in Hulswar. The MEDUSA simulation using the Anderson et al. (2001) parameterization shows oceanic DMS maximising at 11 nM, while when a variable chl-a concentration field is used in the MODIS-DMS simulation, oceanic DMS maximises at 18 nM (64% higher than in the MEDUSA simulation).

To examine how the simulations compare with observations, we compare the oceanic DMS distribution against TAN1802 and SOAP voyages for the regions and times at which those voyages took place (Figure 3, Figure 4). For the TAN1802 voyage (40–70°S, 180°E), the distribution of measured oceanic DMS aligns closely with the Lana simulation. MODIS-DMS and MEDUSA have lower means of 1.19 and 1.52 nM, respectively, but MODIS-DMS has a high CoV of 79% due to higher concentrations at lower latitudes (45 °S) of the Southern Ocean. Oceanic DMS in the Hulswar simulation overestimates DMS concentrations by a factor of two between 45–65 °S.

For the SOAP voyage, which targeted phytoplankton bloom events (42–47°S, 172–180°E), the measured DMS distribution is skewed toward higher concentrations compared with the TAN1802 voyage (Figure 4). In contrast, TAN1802 transected the Southern Ocean without specific focus on bloom activity, yielding a range of DMS concentrations. We consider that SOAP is still useful as it offers insights into extreme conditions not reflected in other data sets. All simulations fail to capture the higher concentrations measured by SOAP. Oceanic DMS in the MODIS-DMS exhibits the highest variability (CoV of 36%), mean, and maximum concentration. MODIS-DMS also aligns best with SOAP, in that it captures some of the high DMS concentrations resulting from phytoplankton blooms. The MODIS-DMS simulation captures around half of the variability of SOAP measurements, whereas the other simulations only match between 7% to 18%. MODIS-DMS is within 11% of the SOAP mean, whereas the other simulations are 22% to 218% lower. See Figure **??** and **??** for simulated comparisons of DMS emission to SOAP and TAN1802.

The Anderson et al. (2001) parameterization assumes chl-a is central to oceanic DMS formation. Previous correlations between chl-a and oceanic DMS, given by the coefficient of determination (R^2), range globally from 0.11 to 0.93, with higher latitudes having increased R^2 values due to factors like nutrient availability and prolonged summer daylight, coupled with heightened wind speeds (Uhlig et al., 2019; Townsend and Keller, 1996; Tison et al., 2010; Matrai et al., 1993). Gros et al. (2023) estimated an R^2 of 0.93 towards sea ice latitudes, while Bell et al. (2021) found chl-a explains just 15% of oceanic DMS variability. Using the Anderson et al. (2001) parameterization in MODIS-DMS, we determined a large R^2 of 0.75 in the Southern Ocean. While associating chl-a with oceanic DMS has discrepancies (Gros et al., 2023; Bell et al., 2021), we show that using Anderson et al. (2001) with satellite chl-a data better represents Southern Ocean summertime DMS compared with the MEDUSA configuration.

Chl-a is used to calculate oceanic DMS in two of the four ESMs with interactive biogeochemistry in CMIP6 (Bock et al., 2021). These models reveal discrepancies between each other and observed oceanic DMS data sets, indicating ongoing uncertainties in CMIP6 ESMs concerning oceanic DMS and its flux to the atmosphere (Bock et al., 2021). Bock et al. (2021) emphasizes the need for enhanced understanding and observations to accurately capture DMS–climate feedbacks. CNRM-

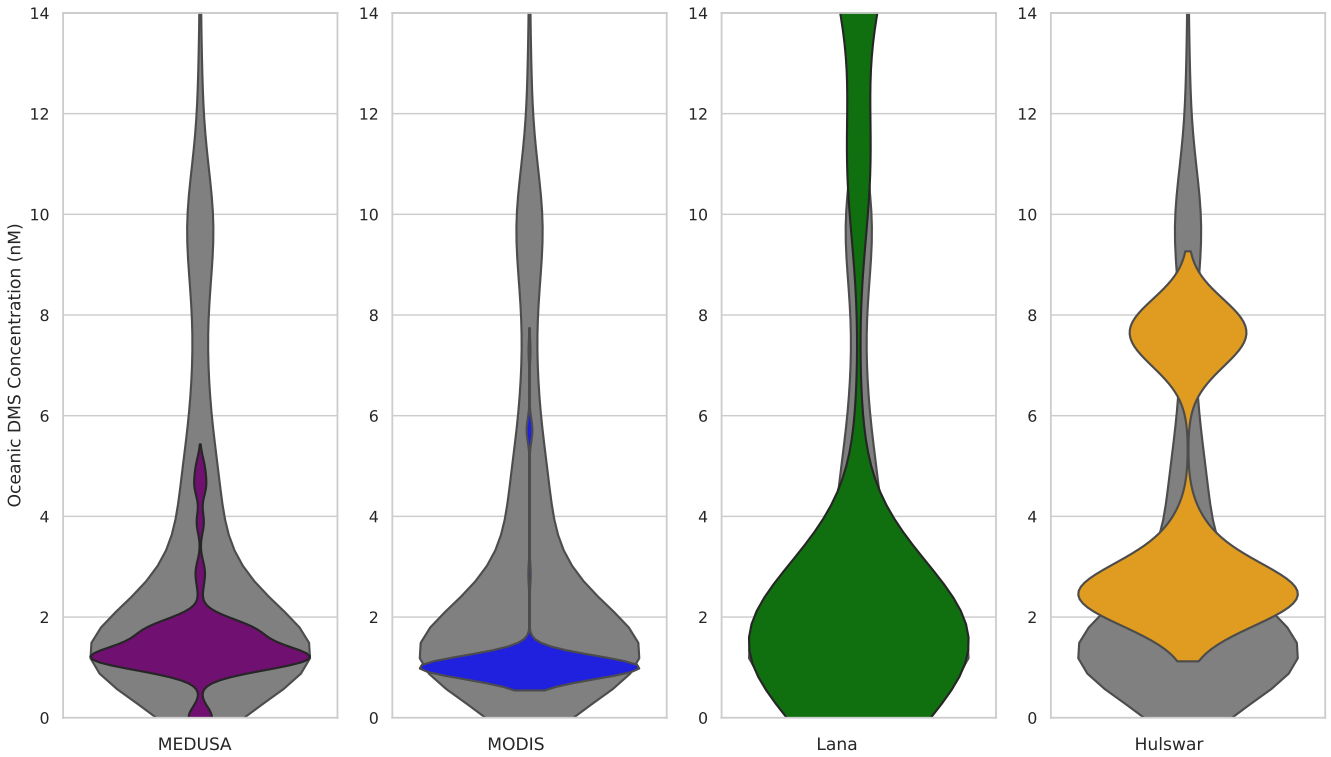

Figure 3. Violin plots of TAN1802 data (grey). Overlaid are the oceanic DMS datasets used in the model simulations (Feb to March 2018, 40 °S to 70 °S, 180 °E) from MEDUSA (purple), MODIS-DMS (blue), Lana (green), and Hulswar (yellow). Violin plots depict data distribution and density. The width of each 'violin' corresponds to the frequency of data points within that value range, while the length indicates the range of values. The frequency axis, represented by the width, allows for an immediate visual comparison of how often particular ranges of values occur in each category. This offers a comprehensive view of both the distribution and frequency of data across different categories.

ESM2-1 adopts an approach considering zooplankton and DMSP rather than chl-a, but its validation is challenging due to limited observational data (Belviso et al., 2012). NorESM2 uses an alternative mechanism for DMS production, by using detritus export production and sea surface temperature (Tjiputra et al., 2020). An oceanic DMS algorithm developed by Galí et al. (2018) includes sea-surface temperature, chl-a, photosynthetically active radiation, and the mixed layer depth, but oceanic DMS has a general overestimation along coastal regions (Galí et al., 2019; Hayashida et al., 2020). Galí et al. (2018) also produced a time series of oceanic DMS over parts of the Northern Hemisphere, finding high inter-annual variability by using chl-a satellite data. Adopting temporally variable oceanic DMS inputs within the model may better reflect inter-annual Southern Ocean variability due to ENSO events and biologically productive years. One such way to achieve this for future projections would be through a stochastic approach of capturing all chl-a years from the satellite (e.g. SeaWiFS and MODIS-aqua) archive.

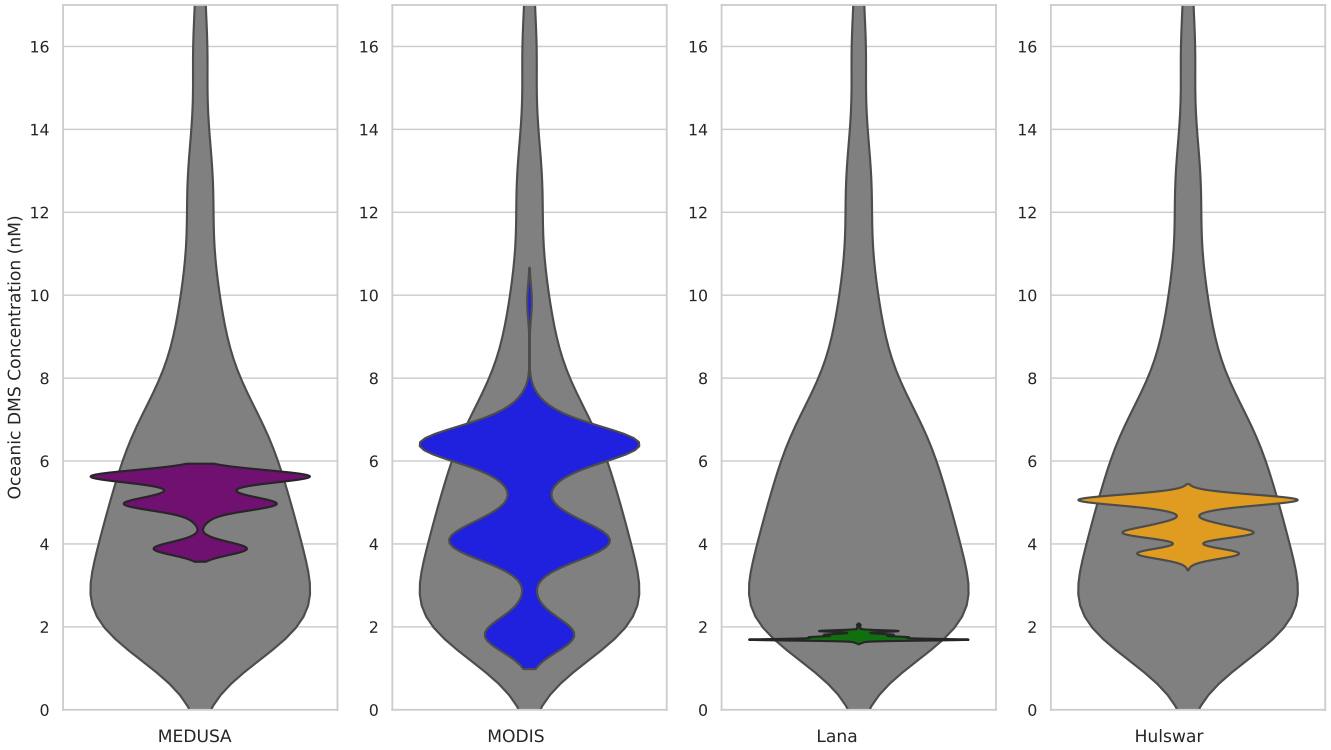

Figure 4. Same as Figure 3, but for the SOAP 2012 voyage (Feb to March 2012, 42–47 °S, 172–180 °E).

3.2 DMS Flux

Having established that oceanic DMS from the MODIS-DMS simulation aligns well with summertime observational voyages as seen in Figure 3, 4, we now assess the sensitivity of atmospheric DMS to various sea-to-air transfer functions (Figure 5, **??**). Figure 5 shows the DMS flux during the austral summer in the Southern Ocean, averaging between 2.9 to 7.3 TgS Yr^{-1}. This is consistent with Jarníková and Tortell (2016) estimation of 3.4 Tg S, aligning most with the MODIS-DMS linear parameterizations (LM86 and B17). The spread in average Southern Ocean summertime DMS fluxes across the eight simulations is 153%, which is greater than the spread between all the simulations testing different oceanic DMS sources, at 107%. The lowest CoVs within both oceanic DMS and DMS emissions are found in the MODIS-DMS simulations, specifically, the Blomquist et al. (2017) parameterization ($MODIS_{B17}$) with a mean of 2.9 $\pm$ 0.84 TgS Yr^{-1}. The upper range of simulated DMS flux, 7.3 $\pm$ 1.8 TgS Yr^{-1}, comes from the W14 quadratic formula used with the Lana DMS climatology ($Lana_{W14}$).

The largest DMS emissions are seen in the $MEDUSA_{LM86}$ simulations, due to the relatively large underlying seawater DMS source spread throughout the Southern Ocean (Figure 2a). The $Lana_{w14}$ simulation also shows large DMS emissions due to the quadratic dependence of the gas transfer velocity on wind speed (Figure 1). Overall, the W14 quadratic formula yields about 33% more emissions than the LM86 and B17 linear formulas. For the transfer velocity parameterizations using a linear

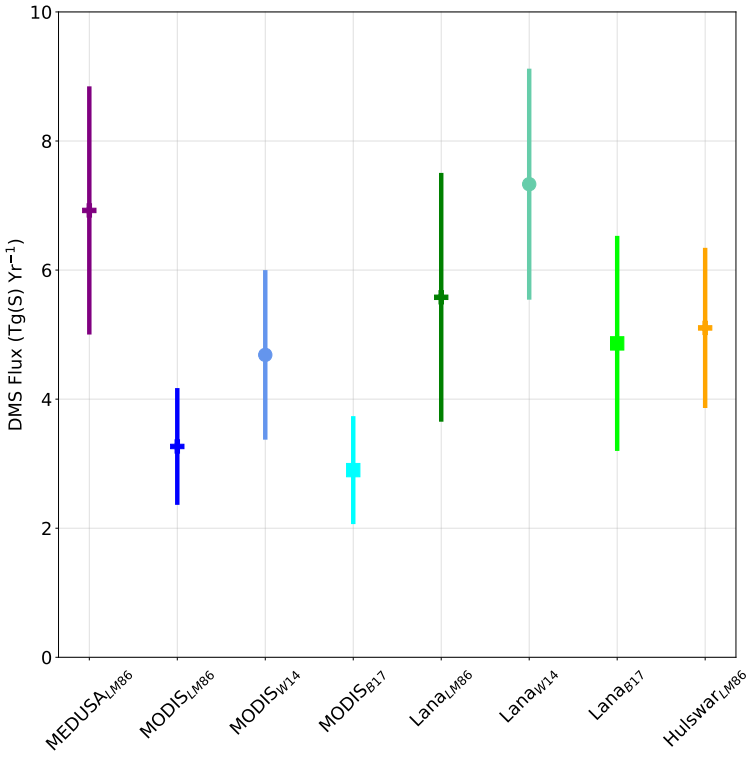

Figure 5. Summertime (December – February) Southern Ocean sulfur emissions in Tg Year^{-1} in all model simulations performed. The error bars represent the spatial and temporal standard deviation. The different colors represent different oceanic DMS climatologies (Purple: MEDUSA ((Sellar et al., 2019; Anderson et al., 2001), Green: (Lana et al., 2011) and Orange: Hulswar ((Hulswar et al., 2022), and time series (Blue: derived from MODIS-DMS chl-a) used in this work. + marker represents simulations performed with the Liss and Merlivat (1986) sea-to-air flux, the dot marker represents Wanninkhof (2014), and the square marker represents Blomquist et al. (2017).

relationship to wind (LM86 and B17), LM86 exhibits a higher transfer velocity than B17 for wind speeds above 7.5 m s^{-1} (Figure 1). Given the Southern Ocean's predominant high wind speeds (Bracegirdle et al., 2020), simulations indicate that LM86 yields 14% more emitted DMS than B17 (Figure 5).

The LM86 flux parameterisation was tested with all oceanic DMS sources, as it is currently the parameterisation used by default in UKESM1-AMIP. Simulations using LM86 have a spread in average summertime Southern Ocean DMS emissions of 112% (3.3 to 6.9 TgS Yr^{-1}). In contrast, simulations using the same oceanic DMS source (MODIS-DMS and Lana) but flux parameterizations (LM86, B17, and W14) have a spread in average summertime Southern Ocean DMS emissions of 51% (MODIS-DMS simulations) to 62% (Lana simulations). The choice of the oceanic DMS source therefore impacts DMS emissions more than the transfer velocity parameterization within these simulations.

Table 3 details simulated daily DMS fluxes over the Western Antarctic Peninsula during the austral summer, for comparison with observations, including Webb et al. (2019). DMS emissions in this period constitute 33-52% of the annual flux, contrasting

Table 3. Mean daily DMS flux over the Western Antarctic Peninsula, by Ryder Bay during the austral summer period for each simulation. The percentage shows the proportions of the total annual DMS flux which occurs during the summer months. Additionally, the total DJF flux shows the mean daily DMS flux (μmol m^{-2} d^{-1}) and standard deviations.

	$MEDUSA_{LM86}$	$MODIS_{LM86}$	$MODIS_{W14}$	$MODIS_{B17}$	$Lana_{LM86}$	$Lana_{W14}$	$Lana_{B17}$	$Hulswar_{LM86}$	Webb et al. (2019)
Total DJF %	44	34	33	36	49	46	52	46	72
Total DJF (μmol m^{-2} d^{-1})	4.3 ± 4	2.2 ± 2.5	2.7 ± 3	1.9 ± 2	5.6 ± 5.1	8.4 ± 7.5	5.3 ± 4.2	6 ± 5.2	29

with the 72% reported by Webb et al. (2019). The region exhibits significant sea-ice melt and high DMS emissions during DJF. Our simulations daily mean flux during DJF is 4.6 ± 4 μmol m^{-2} d^{-1}, below Webb et al. (2019)'s 29 μmol m^{-2} d^{-1} for Ryder Bay (67.54 °S, 68.35 °W). However, our results align with the emissions from Jarníková and Tortell (2016); Berresheim et al. (1998); Asher et al. (2017). Like in Jarníková and Tortell (2016) and Webb et al. (2019), we find periodic hot spots of DMS emissions above 50 μmol m^{-2} d^{-1} over these sub-Antarctic regions, but at 10% the magnitude of the maximum found by Webb et al. (2019).

A 2018 Southern Ocean voyage during February reported a mean daily flux of 2.6 ± 3.5 μmol m^{-2} d^{-1} over the open ocean (Zhang et al., 2020). Our simulations are in good agreement with this, showing DMS fluxes of 2.7 μmol m^{-2} d^{-1} ($MODIS_{B17}$) to 8.9 μmol m^{-2} d^{-1} ($Lana_{W14}$) for the same region and period of time. Shon et al. (2001) estimated a daily flux of 2.6 ± 1.8 μmol m^{-2} d^{-1} around early December. Only the $MODIS_{B17}$ simulation matches these daily fluxes. Furthermore, the linear MODIS-DMS simulations ($MODIS_{LM86}$ and $MODIS_{B17}$) are in good agreement with the 12 ± 15 μmol m^{-2} d^{-1} measured by Marandino et al. (2009) and the 2.8 μmol m^{-2} d^{-1} measured by Lee et al. (2010) in the Southern Ocean.

Many CMIP6 models use the quadratic sea-to-air flux parameterization detailed in Wanninkhof (2014) for DMS emissions (e.g. Salzmann et al., 2022; Seland et al., 2019; Neubauer et al., 2019; Tatebe and Watanabe, 2018; Wu et al., 2019). Yet, recent studies indicate a linear relationship between DMS and wind speed (e.g. Blomquist et al., 2017; Goddijn-Murphy et al., 2016; Bell et al., 2013; Zavarsky et al., 2018; Vlahos and Monahan, 2009; Bell et al., 2015). We demonstrate that linear DMS transfer velocities represent the DMS flux ranges better than the quadratic W14 flux when compared to Southern Ocean observations.

3.3 Atmospheric DMS

We next evaluate atmospheric DMS in our sensitivity simulations. Figure 6 compares all simulated atmospheric DMS with observational datasets. Data in Figure 6 is from three Southern Ocean voyages (SOAP, SOIREE, ANDREXII; Figure 6a-c) and two stations (Cape Grim and King Sejong Station; Figure 6d-e). Figure 6f shows aggregate averaged DMS concentrations from all five observational sources, and has an average summertime concentration of 129 ± 74 ppt (Smith et al., 2018; Wohl et al., 2020; Boyd and Law, 2001, Figure 6f). The simulations using the MODIS-DMS oceanic source and linear DMS transfer models (LM86 and B17) show the closest agreement with the observational mean, of 106 ± 66 ppt and 100 ± 60 ppt for $MODIS_{LM86}$ and $MODIS_{B17}$, respectively. The mean total spread in summertime Southern Ocean atmospheric DMS across all simulations is 171%, compared with the spread of 153% in DMS emissions.

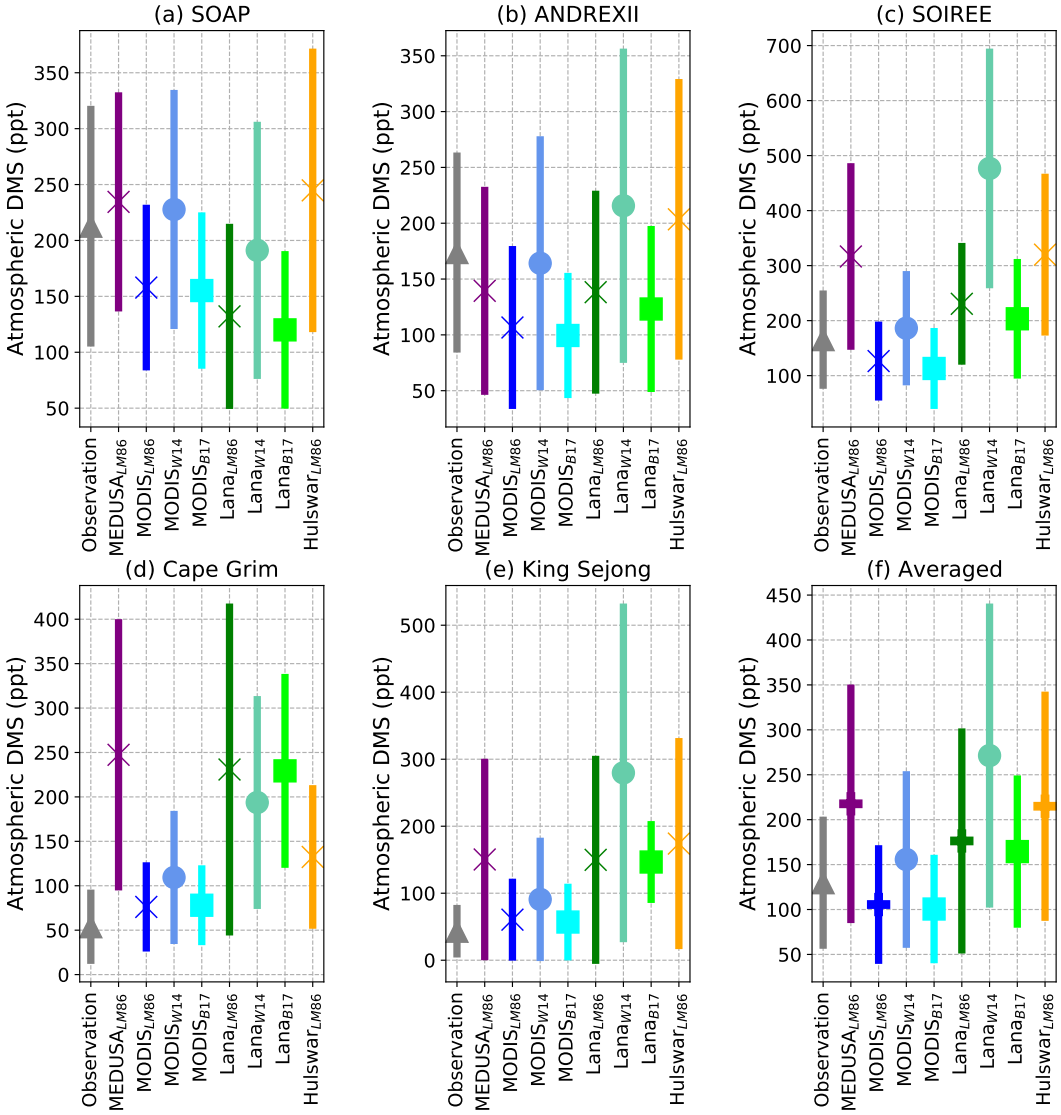

Figure 6. Five observational datasets measuring atmospheric DMS concentrations (ppt) are directly compared with the eight simulations (a – e) at the same spatial and temporal resolution. In (a) SOAP and (b) ANDREXII, we follow both voyages using the nearest grid cell along each hour of the simulations, matching the timescales in 2012 and 2019. For comparing the simulations with the (c) SOIREE voyage, we also follow this voyage in an hourly timescale, but due to the voyage being outside our study period, we average this over all 10 years. The two observational stations used are (d) Cape Grim and (e) King Sejong Station. We calculate the nearest grid-cell for each simulation to the observational station and constructed an average over 10 years along with a temporal standard deviation. From this, we construct an overall average (f) and standard deviation for all observational measurements and simulations which can be compared directly to these observations.

Our simulations, compared to coastal Antarctic measurements, offer insights into the performance of sea ice-influenced regions (Galí et al., 2021). In summer, Berresheim et al. (1998) recorded mean atmospheric DMS of 119 ppt at 64.8 °S, 64 °W, closely matching MODIS$_{B17}$ at 121 ppt. All other DMS sources show concentrations which are more than twice as large as this measurement. Read et al. (2008) measured atmospheric DMS concentrations of 45 $\pm$ 50 ppt at Halley Station, Antarctica (75.4 °S, 26.2 °W), best aligning with Lana$_{B17}$ at 42 ppt. It should be noted that all simulations fall within one standard deviation of the measurements reported at Halley Station. Preunkert et al. (2007) measured high interannual variation of atmospheric DMS at Dumont d'Urville (66.4 °S, 140 °E) during January, from 244 ppt in 2002 to only 60 ppt in 2003. The average January concentration over 13 years was 170 $\pm$ 180 ppt. Here, the Lana and Hulswar simulations are in closest agreement, and simulate average DMS concentrations between 92 and 141 ppt. Lastly, Lee et al. (2010) measured a 61 ppt average over the Pacific Southern Ocean in February, closest to MODIS$_{B17}$ and MODIS$_{LM86}$ (64 and 53 ppt, respectively).

Multi-annual studies emphasize high yearly variability (Read et al., 2008; Preunkert et al., 2007). Measurements during austral summer over the Southern Ocean show significant variability, especially in higher latitudes. The climatologies produce higher concentrations along the coastal regions of Antarctica, as illustrated in Figure 2a-d, but MODIS-DMS still captures much of the spatial variability (Figure **??**). MEDUSA performs the worst over these higher latitude regions, where sea ice can have a large role in producing atmospheric DMS (Galí et al., 2021). MODIS$_{B17}$ represents atmospheric DMS more accurately than models like MEDUSA, Lana, and Hulswar based on observations over the Southern Ocean during summertime.

3.4 Effects from Inter-annual and Spatial Variability

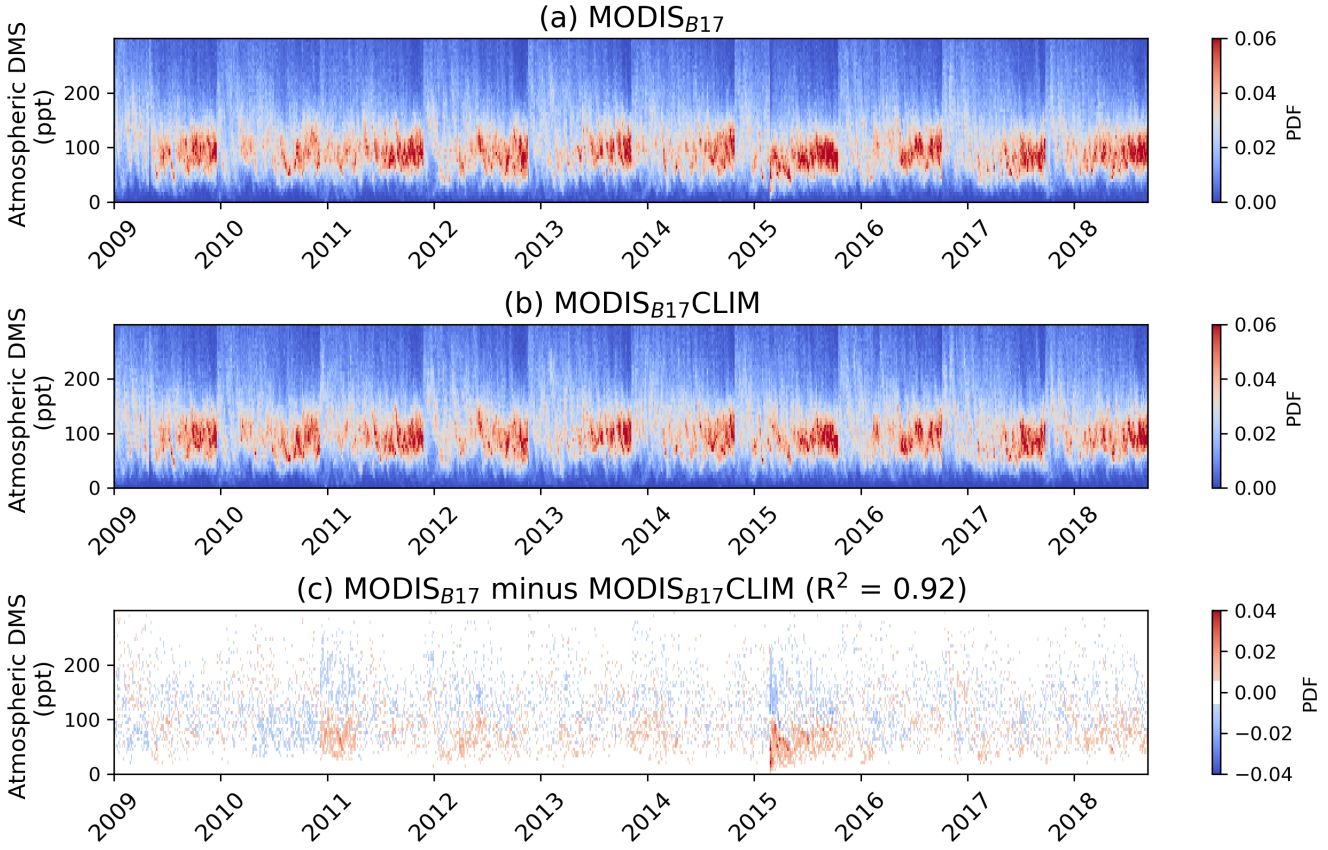

Figure 7. Time series of the atmospheric DMS probability density function between (a) MODIS$_{B17}$ and (b) MODIS$_{B17}$CLIM from 2009 to 2018 summer over the entire Southern Ocean. (c) the difference between MODIS$_{B17}$ and MODIS$_{B17}$CLIM is also shown, with the R^2 shown between the two simulations.

To assess the impact of interannual variability in oceanic DMS on simulated atmospheric DMS, we compare the MODIS$_{B17}$ simulation with MODIS$_{B17}$CLIM, which used a climatology of oceanic DMS calculated from the MODIS-DMS data set (Figure 7). Both simulations are similar (R^2 = 0.92) in terms of interannual variability across the Southern Ocean as a whole. (Figure 7c). Rolling means are presented in Figure **??**b, c. While there are small differences in Southern Ocean atmospheric DMS between the simulations, the overwhelming similarities between Figure 7a and b suggest that an oceanic DMS climatology results in similar interannual variability in the atmospheric DMS PDF suggesting that oceanic DMS is not a strong driver of interannual variability in atmospheric DMS. This result is in contrast to that of Galí et al. (2018) who used a different algorithm for producing oceanic DMS. This difference may be due to our use of the Anderson et al. (2001) algorithm, which is known to produce limited variability (Belviso et al., 2004; Bock et al., 2021).

To assess the impact of spatial variability in oceanic DMS on simulated atmospheric DMS, we compare simulations performed using the MEDUSA and MODIS-DMS data sets (with low and high spatial variability in oceanic DMS, respectively) in Figure 8. Larger variability in the MODIS-DMS oceanic DMS source leads to larger variability in simulated atmospheric DMS, compared with the MEDUSA simulations. The spatial CoV from MEDUSA$_{LM86}$ is 45% lower than MODIS$_{LM86}$, showing greater spatial variability from MODIS-derived chl-a. The oceanic DMS signal in the atmosphere is strong but includes large fluctuations the wind.

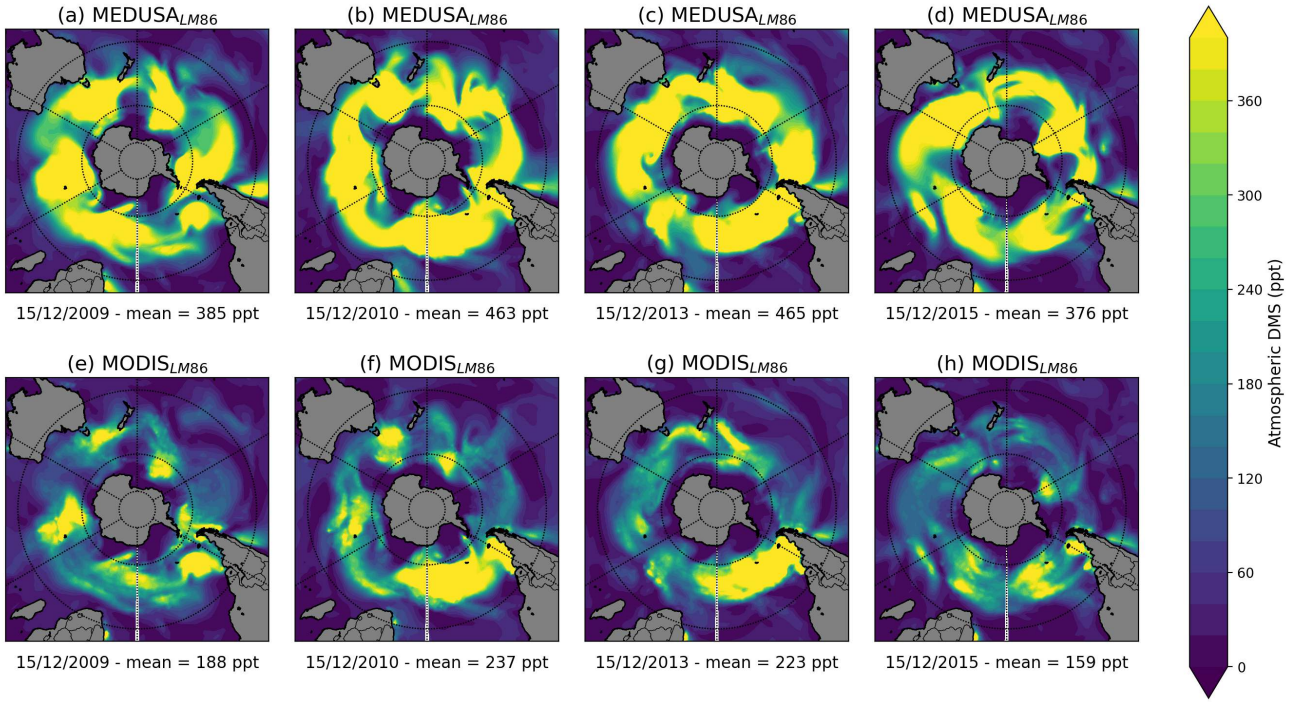

Figure 8. Atmospheric DMS concentrations comparing (a - d) MEDUSA$_{LM86}$ with (e - h) MODIS$_{LM86}$ across four of the same summertime days (15^{th} December) in (a, e) 2009, (b, f) 2010, (c, g) 2013, (d, h) 2015. The area-weighted Southern Ocean mean is shown below each plot.

3.5 Aerosol and cloud response

Figure 9 shows the effect on cloud and aerosol properties of changing the atmospheric DMS distribution. Changing the atmospheric DMS concentration yields little change to CCN, CDNC or AOD. This suggests that these variables are significantly influenced by factors such as sea spray aerosol and the atmospheric oxidation pathways that convert DMS to sulfate aerosol (Revell et al., 2021; Fossum et al., 2020). Changes to the DMS source increase the spread in simulated CCN and CDNC over the Southern Ocean rather than changing the mean DMS emissions, which is consistent with our findings for atmospheric DMS concentrations. Altering the DMS source affects AOD by 73% more than DMS emissions over the Southern Ocean,

emphasizing the role of the ocean in producing atmospheric DMS. Box plots of AOD, CCN, and CDNC (Figure 9e, a, c) show that the simulations do not capture the maxima in CDNC, CCN or AOD over the Southern Ocean.

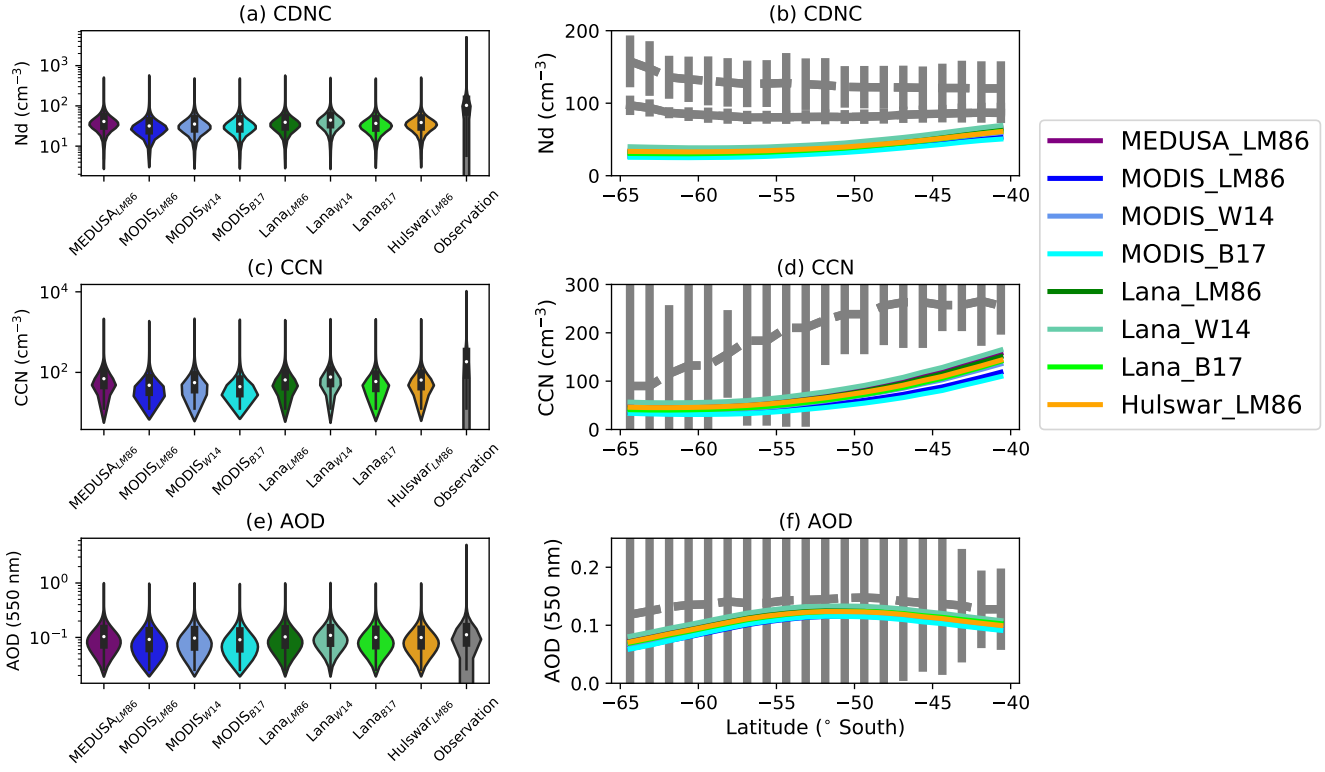

Figure 9. Summertime climatology between 60° S to 40° S showing the (a,b) cloud droplet number concentrations, (c,d) cloud conversation nuclei (800 m in altitude), and (d,e) aerosol optical depth at 550 nm. The violin plots (a,c,e) represent all spatial and temporal data points across the 10 years over the Southern Ocean in DJF. The lowest 1% of values are excluded from the violin plots. In (b,d,f) the grey lines represent observational datasets where (b) Grosvenor et al. (2018) (dashed) and Bennartz and Rausch (2017) (solid) are shown for CDNC, (d) Choudhury and Tesche (2023) is shown at 818m, and (f) AOD climatology by the MODIS satellite-retrieval is shown (Platnick et al., 2017). The error bars represent one standard deviation either side of the observational mean.

4 Conclusions

Modelled atmospheric DMS over the Southern Ocean is sensitive to both oceanic sources and sea-to-air emissions. We examined the sensitivity of atmospheric DMS to different oceanic source data sets and sea-to-air transfer velocity parameterizations using the UKESM1-AMIP model. We also demonstrate the effectiveness of using a 'MODIS-DMS' oceanic DMS data set and climatology calculated from satellite chlorophyll-a observations. MODIS-DMS simulations indicate that large open water areas in the Southern Ocean have lower oceanic DMS concentrations compared to the other three oceanic DMS data sets tested (MEDUSA, Lana, and Hulswar). Climatologies compiled from in-situ observations (Lana and Hulswar) depict fewer distinct

features in oceanic DMS concentrations than MODIS-DMS. Coastal regions have enhanced chlorophyll-a and DMS, and we demonstrate the influence of spatiotemporal chl-a fluctuations on oceanic and atmospheric DMS. Atmospheric DMS in the MODIS-DMS time series simulation shows similar interannual variability to the MODIS-DMS-CLIM simulation, indicating that capturing realistic spatial variability is more important than capturing realistic interannual variability.

Current oceanic DMS climatologies in climate models lack realistic spatial distributions for Southern Ocean summer, evident from voyage comparisons and atmospheric DMS spatial distribution. We show how using chl-a data from the MODIS-aqua satellites offers a good spatial representation of oceanic DMS. Approaches such as this and that of Gali et al offer promising avenues for realistically capturing spatial variability in oceanic DMS associated with marine biogenic activity. The current approach to calculating oceanic DMS within UKESM1 (MEDUSA) shows little spatial variability and high average biases in the Southern Ocean region, emphasizing the need for further refinement (e.g. Bock et al., 2021; Mulcahy et al., 2020; Yool et al., 2021).

We find that atmospheric DMS sensitivity to oceanic DMS changes surpasses the sensitivity to flux parameterizations in our study. Different oceanic DMS concentrations, using the same sea-to-air parameterization, lead to a 112% spread across the means within the DMS emissions. In contrast, changing just the DMS flux parameterization alone results in a 50-60% spread. The total spread in average Southern Ocean DMS emissions across all simulations is 153%, while the atmospheric DMS concentration spread is 171%. Both oceanic DMS and DMS flux parameterization changes significantly influence atmospheric DMS, emphasizing the need for careful consideration in future research.

The Wanninkhof (2014) quadratic DMS parameterization leads to 33% more DMS emissions than Liss and Merlivat (1986) and Blomquist et al. (2017). Linear transfer velocity parameterizations align better with observations for DMS emissions, particularly for the MODIS-DMS simulations. Using a linear flux parameterization within MODIS-DMS brought atmospheric DMS (88 ± 55 ppt) closer to observations (108 ± 61 ppt). In future, we recommend that models use up-to-date DMS-specific relationships such as B17.

Author contributions. Author contributions. YAB implemented model developments, performed model simulations and wrote the manuscript with assistance from all co-authors. LER, AJM and AJS assisted with the experimental design and the model evaluation compared with the observational datasets and sensitivity analysis. ATA advised on DMS chemistry and aerosols over the Southern Ocean. CH provided assistance for lodging DMS emissions into the UKESM1 trunk. JW and EB provided technical expertise in running model simulations.

Competing interests. no competing interests are present

Acknowledgements. This research was supported by the Deep South National Science Challenge (Grant Nos. C01X141E2 and C01X1901) and the UK Met Office for the use of the MetUM. We also acknowledge the contribution of New Zealand eScience Infrastructure (NeSI) high-performance computing facilities to the results of this research. New Zealand's national facilities are provided by NeSI and funded jointly

by NeSI's collaborator institutions and through the Ministry of Business, Innovation and Employment's Research Infrastructure programme (https://www.nesi.org.nz/, last access: 06 April 2023). We acknowledge the Cape Grim Science Program for the provision of DMS data from Cape Grim. The Cape Grim Science Program is a collaboration between the Australian Bureau of Meteorology and CSIRO Australia. LER appreciates support by the Rutherford Discovery Fellowships from New Zealand Government funding, administered by the Royal Society Te Apārangi.

References

Anderson, T., Spall, S., Yool, A., Cipollini, P., Challenor, P., and Fasham, M.: Global fields of sea surface dimethylsulfide predicted from chlorophyll, nutrients and light, Journal of Marine Systems, 30, 1–20, 2001.

Asher, E. C., Dacey, J. W. H., Stukel, M., Long, M. C., and Tortell, P. D.: Processes driving seasonal variability in DMS, DMSP, and DMSO concentrations and turnover in coastal Antarctic waters, Limnology and Oceanography, 62, 104–124, https://doi.org/10.1002/lno.10379, _eprint: https://onlinelibrary.wiley.com/doi/pdf/10.1002/lno.10379, 2017.

Bates, T. S., Cline, J. D., Gammon, R. H., and Kelly-Hansen, S. R.: Regional and seasonal variations in the flux of oceanic dimethylsulfide to the atmosphere, Journal of Geophysical Research: Oceans, 92, 2930–2938, publisher: Wiley Online Library, 1987.

Behrens, E. and Bostock, H.: The Response of the Subtropical Front to Changes in the Southern Hemisphere Westerly Winds—Evidence From Models and Observations, Journal of Geophysical Research: Oceans, 128, e2022JC019 139, publisher: Wiley Online Library, 2023.

Bell, T., De Bruyn, W., Miller, S., Ward, B., Christensen, K., and Saltzman, E.: Air–sea dimethylsulfide (DMS) gas transfer in the North Atlantic: evidence for limited interfacial gas exchange at high wind speed, Atmospheric Chemistry and Physics, 13, 11 073–11 087, publisher: Copernicus GmbH, 2013.

Bell, T., De Bruyn, W., Marandino, C. A., Miller, S., Law, C., Smith, M., and Saltzman, E.: Dimethylsulfide gas transfer coefficients from algal blooms in the Southern Ocean, Atmospheric Chemistry and Physics, 15, 1783–1794, publisher: Copernicus GmbH, 2015.

Bell, T. G., Porter, J. G., Wang, W.-L., Lawler, M. J., Boss, E., Behrenfeld, M. J., and Saltzman, E. S.: Predictability of Seawater DMS During the North Atlantic Aerosol and Marine Ecosystem Study (NAAMES), Frontiers in Marine Science, 7, 596 763, publisher: Frontiers Media SA, 2021.

Belviso, S., Bopp, L., Moulin, C., Orr, J. C., Anderson, T., Aumont, O., Chu, S., Elliott, S., Maltrud, M. E., and Simó, R.: Comparison of global climatological maps of sea surface dimethyl sulfide, Global Biogeochemical Cycles, 18, https://doi.org/10.1029/2003GB002193, publisher: American Geophysical Union, 2004.

Belviso, S., Masotti, I., Tagliabue, A., Bopp, L., Brockmann, P., Fichot, C., Caniaux, G., Prieur, L., Ras, J., Uitz, J., Loisel, H., Dessailly, D., Alvain, S., Kasamatsu, N., and Fukuchi, M.: DMS dynamics in the most oligotrophic subtropical zones of the global ocean, Biogeochemistry, 110, 215–241, https://doi.org/10.1007/s10533-011-9648-1, 2012.

Bennartz, R. and Rausch, J.: Global and regional estimates of warm cloud droplet number concentration based on 13 years of AQUA-MODIS observations, Atmospheric Chemistry and Physics, 17, 9815–9836, https://doi.org/10.5194/acp-17-9815-2017, publisher: Copernicus GmbH, 2017.

Berresheim, H., Huey, J., Thorn, R., Eisele, F., Tanner, D., and Jefferson, A.: Measurements of dimethyl sulfide, dimethyl sulfoxide, dimethyl sulfone, and aerosol ions at Palmer Station, Antarctica, Journal of Geophysical Research: Atmospheres, 103, 1629–1637, publisher: Wiley Online Library, 1998.

Bhatti, Y. A., Revell, L. E., and McDonald, A. J.: Influences of Antarctic ozone depletion on Southern Ocean aerosols, Journal of Geophysical Research: Atmospheres, 127, e2022JD037 199, publisher: Wiley Online Library, 2022.

Blomquist, B. W., Brumer, S. E., Fairall, C. W., Huebert, B. J., Zappa, C. J., Brooks, I. M., Yang, M., Bariteau, L., Prytherch, J., Hare, J. E., and others: Wind speed and sea state dependencies of air-sea gas transfer: Results from the High Wind speed Gas exchange Study (HiWinGS), Journal of Geophysical Research: Oceans, 122, 8034–8062, publisher: Wiley Online Library, 2017.

Bock, J., Michou, M., Nabat, P., Abe, M., Mulcahy, J. P., Olivié, D. J., Schwinger, J., Suntharalingam, P., Tjiputra, J., Van Hulten, M., and others: Evaluation of ocean dimethylsulfide concentration and emission in CMIP6 models, Biogeosciences, 18, 3823–3860, publisher: Copernicus GmbH, 2021.

Boyd, P. and Law, C.: The Southern Ocean iron release experiment (SOIREE)—introduction and summary, Deep Sea Research Part II: Topical Studies in Oceanography, 48, 2425–2438, publisher: Elsevier, 2001.

Bracegirdle, T., Holmes, C., Hosking, J., Marshall, G., Osman, M., Patterson, M., and Rackow, T.: Improvements in circumpolar Southern Hemisphere extratropical atmospheric circulation in CMIP6 compared to CMIP5, Earth and Space Science, 7, e2019EA001 065, 2020.

Browning, T. J., Stone, K., Bouman, H. A., Mather, T. A., Pyle, D. M., Moore, C. M., and Martinez-Vicente, V.: Volcanic ash supply to the surface ocean—remote sensing of biological responses and their wider biogeochemical significance, Frontiers in Marine Science, 2, 14, publisher: Frontiers Media SA, 2015.

Choudhury, G. and Tesche, M.: A first global height-resolved cloud condensation nuclei data set derived from spaceborne lidar measurements, Earth System Science Data, 15, 3747–3760, https://doi.org/10.5194/essd-15-3747-2023, publisher: Copernicus GmbH, 2023.

Curson, A. R. J., Todd, J. D., Sullivan, M. J., and Johnston, A. W. B.: Catabolism of dimethylsulphoniopropionate: microorganisms, enzymes and genes, Nature Reviews Microbiology, 9, 849–859, https://doi.org/10.1038/nrmicro2653, number: 12 Publisher: Nature Publishing Group, 2011.

Deppeler, S. L. and Davidson, A. T.: Southern Ocean phytoplankton in a changing climate, Frontiers in Marine Science, 4, 40, publisher: Frontiers Media SA, 2017.

Elliott, S.: Dependence of DMS global sea-air flux distribution on transfer velocity and concentration field type, Journal of Geophysical Research: Biogeosciences, 114, publisher: Wiley Online Library, 2009.

Fairall, C., Yang, M., Bariteau, L., Edson, J., Helmig, D., McGillis, W., Pezoa, S., Hare, J., Huebert, B., and Blomquist, B.: Implementation of the Coupled Ocean-Atmosphere Response Experiment flux algorithm with CO2, dimethyl sulfide, and O3, Journal of Geophysical Research: Oceans, 116, publisher: Wiley Online Library, 2011.

Fossum, K. N., Ovadnevaite, J., Ceburnis, D., Preißler, J., Snider, J. R., Huang, R.-J., Zuend, A., and O'Dowd, C.: Sea-spray regulates sulfate cloud droplet activation over oceans, npj Climate and Atmospheric Science, 3, 1–6, https://doi.org/10.1038/s41612-020-0116-2, number: 1 Publisher: Nature Publishing Group, 2020.

Galí, M., Levasseur, M., Devred, E., Simó, R., and Babin, M.: Sea-surface dimethylsulfide (DMS) concentration from satellite data at global and regional scales, Biogeosciences, 15, 3497–3519, publisher: Copernicus GmbH, 2018.

Galí, M., Devred, E., Babin, M., and Levasseur, M.: Decadal increase in Arctic dimethylsulfide emission, Proceedings of the National Academy of Sciences, 116, 19 311–19 317, publisher: National Acad Sciences, 2019.

Galí, M., Lizotte, M., Kieber, D. J., Randelhoff, A., Hussherr, R., Xue, L., Dinasquet, J., Babin, M., Rehm, E., and Levasseur, M.: DMS emissions from the Arctic marginal ice zone, Elem Sci Anth, 9, 00 113, publisher: University of California Press, 2021.

Goddijn-Murphy, L., Woolf, D. K., Callaghan, A. H., Nightingale, P. D., and Shutler, J. D.: A reconciliation of empirical and mechanistic models of the air-sea gas transfer velocity, Journal of Geophysical Research: Oceans, 121, 818–835, publisher: Wiley Online Library, 2016.

Gregg, W. W. and Casey, N. W.: Sampling biases in MODIS and SeaWiFS ocean chlorophyll data, Remote Sensing of Environment, 111, 25–35, publisher: Elsevier, 2007.

Gros, V., Bonsang, B., Sarda-Estève, R., Nikolopoulos, A., Metfies, K., Wietz, M., and Peeken, I.: Concentrations of dissolved dimethyl sulfide (DMS), methanethiol and other trace gases in context of microbial communities from the temperate Atlantic to the Arctic Ocean, Biogeosciences, 20, 851–867, https://doi.org/10.5194/bg-20-851-2023, publisher: Copernicus GmbH, 2023.

Grosvenor, D. P., Sourdeval, O., Zuidema, P., Ackerman, A., Alexandrov, M. D., Bennartz, R., Boers, R., Cairns, B., Chiu, J. C., Christensen, M., Deneke, H., Diamond, M., Feingold, G., Fridlind, A., Hünerbein, A., Knist, C., Kollias, P., Marshak, A., McCoy, D., Merk, D., Painemal, D., Rausch, J., Rosenfeld, D., Russchenberg, H., Seifert, P., Sinclair, K., Stier, P., van Diedenhoven, B., Wendisch, M., Werner, F., Wood, R., Zhang, Z., and Quaas, J.: Remote Sensing of Droplet Number Concentration in Warm Clouds: A Review of the Current State of Knowledge and Perspectives, Reviews of Geophysics, 56, 409–453, https://doi.org/10.1029/2017RG000593, _eprint: https://onlinelibrary.wiley.com/doi/pdf/10.1029/2017RG000593, 2018.

Hajima, T., Watanabe, M., Yamamoto, A., Tatebe, H., Noguchi, M. A., Abe, M., Ohgaito, R., Ito, A., Yamazaki, D., Okajima, H., and others: Development of the MIROC-ES2L Earth system model and the evaluation of biogeochemical processes and feedbacks, Geoscientific Model Development, 13, 2197–2244, publisher: Copernicus GmbH, 2020.

Hayashida, H., Carnat, G., Galí, M., Monahan, A. H., Mortenson, E., Sou, T., and Steiner, N. S.: Spatiotemporal variability in modeled bottom ice and sea surface dimethylsulfide concentrations and fluxes in the Arctic during 1979–2015, Global Biogeochemical Cycles, 34, e2019GB006 456, publisher: Wiley Online Library, 2020.

Haëntjens, N., Boss, E., and Talley, L. D.: Revisiting O cean C olor algorithms for chlorophyll a and particulate organic carbon in the S outhern O cean using biogeochemical floats, Journal of Geophysical Research: Oceans, 122, 6583–6593, publisher: Wiley Online Library, 2017.

Hersbach, H., Bell, B., Berrisford, P., Hirahara, S., Horányi, A., Muñoz-Sabater, J., Nicolas, J., Peubey, C., Radu, R., Schepers, D., and others: The ERA5 global reanalysis, Quarterly Journal of the Royal Meteorological Society, 146, 1999–2049, publisher: Wiley Online Library, 2020.

Hu, C., Feng, L., Lee, Z., Franz, B. A., Bailey, S. W., Werdell, P. J., and Proctor, C. W.: Improving satellite global chlorophyll a data products through algorithm refinement and data recovery, Journal of Geophysical Research: Oceans, 124, 1524–1543, publisher: Wiley Online Library, 2019.

Huebert, B. J., Blomquist, B. W., Yang, M. X., Archer, S. D., Nightingale, P. D., Yelland, M. J., Stephens, J., Pascal, R. W., and Moat, B. I.: Linearity of DMS transfer coefficient with both friction velocity and wind speed in the moderate wind speed range, Geophysical Research Letters, 37, https://doi.org/10.1029/2009GL041203, _eprint: https://onlinelibrary.wiley.com/doi/pdf/10.1029/2009GL041203, 2010.

Hulswar, S., Simó, R., Gali Tapias, M., Bell, T. G., Lana, A., Inamdar, S., Halloran, P. R., Manville, G., and Mahajan, A. S.: Third revision of the global surface seawater dimethyl sulfide climatology (DMS-Rev3), Earth System Science Data, 14, 2963–2987, publisher: Copernicus Publications, 2022.

Jarníková, T. and Tortell, P. D.: Towards a revised climatology of summertime dimethylsulfide concentrations and sea–air fluxes in the Southern Ocean, Environmental Chemistry, 13, 364, https://doi.org/10.1071/EN14272, 2016.

Jena, B.: The effect of phytoplankton pigment composition and packaging on the retrieval of chlorophyll-a concentration from satellite observations in the Southern Ocean, International Journal of Remote Sensing, 38, 3763–3784, publisher: Taylor & Francis, 2017.

Johnson, R., Strutton, P. G., Wright, S. W., McMinn, A., and Meiners, K. M.: Three improved satellite chlorophyll algorithms for the Southern Ocean, Journal of Geophysical Research: Oceans, 118, 3694–3703, publisher: Wiley Online Library, 2013.

Keller, M. D., Bellows, W. K., and Guillard, R. R.: Dimethyl sulfide production in marine phytoplankton, ACS Publications, 1989.

Kettle, A., Andreae, M. O., Amouroux, D., Andreae, T., Bates, T., Berresheim, H., Bingemer, H., Boniforti, R., Curran, M., DiTullio, G., and others: A global database of sea surface dimethylsulfide (DMS) measurements and a procedure to predict sea surface DMS as a function of latitude, longitude, and month, Global Biogeochemical Cycles, 13, 399–444, publisher: Wiley Online Library, 1999.

Kiene, R. P. and Bates, T. S.: Biological removal of dimethyl sulphide from sea water, Nature, 345, 702–705, 1990.

Kloster, S., Feichter, J., Maier-Reimer, E., Six, K. D., Stier, P., and Wetzel, P.: DMS cycle in the marine ocean-atmosphere system–a global model study, Biogeosciences, 3, 29–51, publisher: Copernicus GmbH, 2006.

Korhonen, H., Carslaw, K. S., Spracklen, D. V., Mann, G. W., and Woodhouse, M. T.: Influence of oceanic dimethyl sulfide emissions on cloud condensation nuclei concentrations and seasonality over the remote Southern Hemisphere oceans: A global model study, Journal of Geophysical Research, 113, https://doi.org/10.1029/2007jd009718, 2008.

Kremser, S., Harvey, M., Kuma, P., Hartery, S., Saint-Macary, A., McGregor, J., Schuddeboom, A., Von Hobe, M., Lennartz, S. T., Geddes, A., and others: Southern Ocean cloud and aerosol data: a compilation of measurements from the 2018 Southern Ocean Ross Sea Marine Ecosystems and Environment voyage, Earth System Science Data, 13, 3115–3153, publisher: Copernicus GmbH, 2021.

Kuma, P., McDonald, A. J., Morgenstern, O., Alexander, S. P., Cassano, J. J., Garrett, S., Halla, J., Hartery, S., Harvey, M. J., Parsons, S., and others: Evaluation of Southern Ocean cloud in the HadGEM3 general circulation model and MERRA-2 reanalysis using ship-based observations, Atmospheric Chemistry and Physics, 20, 6607–6630, publisher: Copernicus GmbH, 2020.

Lana, A., Bell, T., Simó, R., Vallina, S., Ballabrera-Poy, J., Kettle, A., Dachs, J., Bopp, L., Saltzman, E., Stefels, J., and others: An updated climatology of surface dimethlysulfide concentrations and emission fluxes in the global ocean, Global Biogeochemical Cycles, 25, publisher: Wiley Online Library, 2011.

Law, C. S., Smith, M. J., Harvey, M. J., Bell, T. G., Cravigan, L. T., Elliott, F. C., Lawson, S. J., Lizotte, M., Marriner, A., McGregor, J., and others: Overview and preliminary results of the Surface Ocean Aerosol Production (SOAP) campaign, Atmospheric Chemistry and Physics, 17, 13 645–13 667, publisher: Copernicus GmbH, 2017.

Lee, G., Park, J., Jang, Y., Lee, M., Kim, K.-R., Oh, J.-R., Kim, D., Yi, H.-I., and Kim, T.-Y.: Vertical variability of seawater DMS in the South Pacific Ocean and its implication for atmospheric and surface seawater DMS, Chemosphere, 78, 1063–1070, publisher: Elsevier, 2010.

Liss, P. S. and Merlivat, L.: Air-sea gas exchange rates: Introduction and synthesis, in: The role of air-sea exchange in geochemical cycling, pp. 113–127, Springer, 1986.

Longman, J., Palmer, M. R., Gernon, T. M., Manners, H. R., and Jones, M. T.: Subaerial volcanism is a potentially major contributor to oceanic iron and manganese cycles, Communications Earth & Environment, 3, 60, publisher: Nature Publishing Group UK London, 2022.

Marandino, C., De Bruyn, W. J., Miller, S., and Saltzman, E.: Open ocean DMS air/sea fluxes over the eastern South Pacific Ocean, Atmospheric Chemistry and Physics, 9, 345–356, publisher: Copernicus GmbH, 2009.

Matrai, P. A., Balch, W. M., Cooper, D. J., and Saltzman, E. S.: Ocean color and atmospheric dimethyl sulfide: on their mesoscale variability, Journal of Geophysical Research: Atmospheres, 98, 23 469–23 476, publisher: Wiley Online Library, 1993.

Mulcahy, J. P., Johnson, C., Jones, C. G., Povey, A. C., Scott, C. E., Sellar, A., Turnock, S. T., Woodhouse, M. T., Abraham, N. L., and Andrews, M. B.: Description and evaluation of aerosol in UKESM1 and HadGEM3-GC3. 1 CMIP6 historical simulations, Geoscientific Model Development, 13, 6383–6423, 2020.

Myhre, G., Shindell, D., and Pongratz, J.: Anthropogenic and natural radiative forcing, publisher: Cambridge University Press, 2014.

Neubauer, D., Ferrachat, S., Siegenthaler-Le Drian, C., Stoll, J., Folini, D., Tegen, I., Wieners, K., Mauritsen, T., Stemmler, I., Barthel, S., and others: HAMMOZ-Consortium MPI-ESM1. 2-HAM model output prepared for CMIP6 AerChemMIP, Earth System Grid Federation, 2019.

Nightingale, P. D., Malin, G., Law, C. S., Watson, A. J., Liss, P. S., Liddicoat, M. I., Boutin, J., and Upstill-Goddard, R. C.: In situ evaluation of air-sea gas exchange parameterizations using novel conservative and volatile tracers, Global Biogeochemical Cycles, 14, 373–387, publisher: Wiley Online Library, 2000.

O'Reilly, J. E. and Werdell, P. J.: Chlorophyll algorithms for ocean color sensors-OC4, OC5 & OC6, Remote sensing of environment, 229, 32–47, publisher: Elsevier, 2019.

Pandis, S. N., Russell, L. M., and Seinfeld, J. H.: The relationship between DMS flux and CCN concentration in remote marine regions, Journal of Geophysical Research: Atmospheres, 99, 16 945–16 957, publisher: Wiley Online Library, 1994.

Pithan, F., Athanase, M., Dahlke, S., Sánchez-Benítez, A., Shupe, M. D., Sledd, A., Streffing, J., Svensson, G., and Jung, T.: Nudging allows direct evaluation of coupled climate models with in-situ observations: A case study from the MOSAiC expedition, EGUsphere, pp. 1–23, publisher: Copernicus GmbH, 2022.

Platnick, S., Meyer, K. G., King, M. D., Wind, G., Amarasinghe, N., Marchant, B., Arnold, G. T., Zhang, Z., Hubanks, P. A., Holz, R. E., Yang, P., Ridgway, W. L., and Riedi, J.: The MODIS cloud optical and microphysical products: Collection 6 updates and examples from Terra and Aqua, IEEE transactions on geoscience and remote sensing : a publication of the IEEE Geoscience and Remote Sensing Society, 55, 502–525, https://doi.org/10.1109/TGRS.2016.2610522, 2017.

Preunkert, S., Legrand, M., Jourdain, B., Moulin, C., Belviso, S., Kasamatsu, N., Fukuchi, M., and Hirawake, T.: Interannual variability of dimethylsulfide in air and seawater and its atmospheric oxidation by-products (methanesulfonate and sulfate) at Dumont d'Urville, coastal Antarctica (1999–2003), Journal of Geophysical Research: Atmospheres, 112, https://doi.org/10.1029/2006JD007585, _eprint: https://onlinelibrary.wiley.com/doi/pdf/10.1029/2006JD007585, 2007.

Read, K., Lewis, A., Bauguitte, S., Rankin, A. M., Salmon, R., Wolff, E. W., Saiz-Lopez, A., Bloss, W., Heard, D., Lee, J., and others: DMS and MSA measurements in the Antarctic Boundary Layer: impact of BrO on MSA production, Atmospheric Chemistry and Physics, 8, 2985–2997, publisher: Copernicus GmbH, 2008.

Revell, L. E., Kremser, S., Hartery, S., Harvey, M., Mulcahy, J. P., Williams, J., Morgenstern, O., McDonald, A. J., Varma, V., and Bird, L.: The sensitivity of Southern Ocean aerosols and cloud microphysics to sea spray and sulfate aerosol production in the HadGEM3-GA7. 1 chemistry–climate model, Atmospheric Chemistry and Physics, 19, 15 447–15 466, 2019.

Revell, L. E., Wotherspoon, N., Jones, O., Bhatti, Y. A., Williams, J., Mackie, S., and Mulcahy, J.: Atmosphere-Ocean Feedback From Wind-Driven Sea Spray Aerosol Production, Geophysical Research Letters, 48, e2020GL091 900, 2021.

Saltzman, E., King, D., Holmen, K., and Leck, C.: Experimental determination of the diffusion coefficient of dimethylsulfide in water, Journal of Geophysical Research: Oceans, 98, 16 481–16 486, publisher: Wiley Online Library, 1993.

Salzmann, M., Ferrachat, S., Tully, C., Münch, S., Watson-Parris, D., Neubauer, D., Siegenthaler-Le Drian, C., Rast, S., Heinold, B., Crueger, T., and others: The Global Atmosphere-aerosol Model ICON-A-HAM2. 3–Initial Model Evaluation and Effects of Radiation Balance Tuning on Aerosol Optical Thickness, Journal of Advances in Modeling Earth Systems, 14, e2021MS002 699, publisher: Wiley Online Library, 2022.

Santoso, A., Mcphaden, M. J., and Cai, W.: The defining characteristics of ENSO extremes and the strong 2015/2016 El Niño, Reviews of Geophysics, 55, 1079–1129, publisher: Wiley Online Library, 2017.

Seland, O., Bentsen, M., Oliviè, D. J. L., Toniazzo, T., Gjermundsen, A., Graff, L. S., Debernard, J. B., Gupta, A. K., He, Y., Kirkevåg, A., and others: NCC NorESM2-LM model output prepared for CMIP6 CMIP historical, Earth System Grid Federation, 10, 2019.

Seland, O., Bentsen, M., Olivié, D., Toniazzo, T., Gjermundsen, A., Graff, L. S., Debernard, J. B., Gupta, A. K., He, Y.-C., Kirkevåg, A., and others: Overview of the Norwegian Earth System Model (NorESM2) and key climate response of CMIP6 DECK, historical, and scenario simulations, Geoscientific Model Development, 13, 6165–6200, publisher: Copernicus GmbH, 2020.

Sellar, A. A., Jones, C. G., Mulcahy, J. P., Tang, Y., Yool, A., Wiltshire, A., O'connor, F. M., Stringer, M., Hill, R., and Palmieri, J.: UKESM1: Description and evaluation of the UK Earth System Model, Journal of Advances in Modeling Earth Systems, 11, 4513–4558, 2019.

Shon, Z.-H., Davis, D., Chen, G., Grodzinsky, G., Bandy, A., Thornton, D., Sandholm, S., Bradshaw, J., Stickel, R., Chameides, W., and others: Evaluation of the DMS flux and its conversion to SO2 over the southern ocean, Atmospheric Environment, 35, 159–172, publisher: Elsevier, 2001.

Smith, M. J., Walker, C. F., Bell, T. G., Harvey, M. J., Saltzman, E. S., and Law, C. S.: Gradient flux measurements of sea–air DMS transfer during the Surface Ocean Aerosol Production (SOAP) experiment, Atmospheric Chemistry and Physics, 18, 5861–5877, https://doi.org/10.5194/acp-18-5861-2018, 2018.

Séférian, R., Nabat, P., Michou, M., Saint-Martin, D., Voldoire, A., Colin, J., Decharme, B., Delire, C., Berthet, S., Chevallier, M., and others: Evaluation of CNRM earth system model, CNRM-ESM2-1: Role of earth system processes in present-day and future climate, Journal of Advances in Modeling Earth Systems, 11, 4182–4227, publisher: Wiley Online Library, 2019.

Tang, W., Llort, J., Weis, J., Perron, M. M., Basart, S., Li, Z., Sathyendranath, S., Jackson, T., Sanz Rodriguez, E., Proemse, B. C., and others: Widespread phytoplankton blooms triggered by 2019–2020 Australian wildfires, Nature, 597, 370–375, publisher: Nature Publishing Group, 2021.

Tang, Y., Rumbold, S., Ellis, R., Kelley, D., Mulcahy, J., Sellar, A., Walton, J., and Jones, C.: MOHC UKESM1. 0-LL model output prepared for CMIP6 CMIP, publisher: World Data Center for Climate (WDCC) at DKRZ, 2019.

Tatebe, H. and Watanabe, M.: MIROC MIROC6 model output prepared for CMIP6 CMIP historical, https://doi.org/10.22033/ESGF/CMIP6.5603, 2018.

Telford, P., Braesicke, P., Morgenstern, O., and Pyle, J.: Description and assessment of a nudged version of the new dynamics Unified Model, Atmospheric Chemistry and Physics, 8, 1701–1712, publisher: Copernicus GmbH, 2008.

Thompson, P. A., Bonham, P., Thomson, P., Rochester, W., Doblin, M. A., Waite, A. M., Richardson, A., and Rousseaux, C. S.: Climate variability drives plankton community composition changes: The 2010–2011 El Niño to La Niña transition around Australia, Journal of Plankton Research, 37, 966–984, publisher: Oxford University Press, 2015.

Tison, J.-L., Brabant, F., Dumont, I., and Stefels, J.: High-resolution dimethyl sulfide and dimethylsulfoniopropionate time series profiles in decaying summer first-year sea ice at Ice Station Polarstern, western Weddell Sea, Antarctica, Journal of Geophysical Research: Biogeosciences, 115, publisher: Wiley Online Library, 2010.

Titchner, H. A. and Rayner, N. A.: The Met Office Hadley Centre sea ice and sea surface temperature data set, version 2: 1. Sea ice concentrations, Journal of Geophysical Research: Atmospheres, 119, 2864–2889, publisher: Wiley Online Library, 2014.

Tjiputra, J. F., Schwinger, J., Bentsen, M., Morée, A. L., Gao, S., Bethke, I., Heinze, C., Goris, N., Gupta, A., He, Y.-C., and others: Ocean biogeochemistry in the Norwegian Earth System Model version 2 (NorESM2), Geoscientific Model Development, 13, 2393–2431, publisher: Copernicus GmbH, 2020.

Townsend, D. W. and Keller, M. D.: Dimethylsulfide (DMS) and dimethylsulfoniopropionate (DMSP) in relation to phytoplankton in the Gulf of Maine, Marine Ecology Progress Series, 137, 229–241, 1996.

Uhlig, C., Damm, E., Peeken, I., Krumpen, T., Rabe, B., Korhonen, M., and Ludwichowski, K.-U.: Sea ice and water mass influence dimethylsulfide concentrations in the central Arctic Ocean, Frontiers in Earth Science, 7, 179, publisher: Frontiers Media SA, 2019.

Vlahos, P. and Monahan, E. C.: A generalized model for the air-sea transfer of dimethyl sulfide at high wind speeds, Geophysical Research Letters, 36, https://doi.org/10.1029/2009gl040695, 2009.

Wang, Y., Chen, H.-H., Tang, R., He, D., Lee, Z., Xue, H., Wells, M., Boss, E., and Chai, F.: Australian fire nourishes ocean phytoplankton bloom, Science of The Total Environment, 807, 150 775, publisher: Elsevier, 2022.

Wanninkhof, R.: Relationship between wind speed and gas exchange over the ocean, Journal of Geophysical Research: Oceans, 97, 7373–7382, https://doi.org/10.1029/92JC00188, 1992.

Wanninkhof, R.: Relationship between wind speed and gas exchange over the ocean revisited, Limnology and Oceanography: Methods, 12, 351–362, https://doi.org/10.4319/lom.2014.12.351, 2014.

Webb, A. v., Van Leeuwe, M., Den Os, D., Meredith, M., J Venables, H., and Stefels, J.: Extreme spikes in DMS flux double estimates of biogenic sulfur export from the Antarctic coastal zone to the atmosphere, Scientific reports, 9, 1–11, publisher: Nature Publishing Group, 2019.

Wohl, C., Brown, I., Kitidis, V., Jones, A. E., Sturges, W. T., Nightingale, P. D., and Yang, M.: Underway seawater and atmospheric measurements of volatile organic compounds in the Southern Ocean, Biogeosciences, 17, 2593–2619, publisher: Copernicus GmbH, 2020.

Wu, T., Lu, Y., Fang, Y., Xin, X., Li, L., Li, W., Jie, W., Zhang, J., Liu, Y., Zhang, L., Zhang, F., Zhang, Y., Wu, F., Li, J., Chu, M., Wang, Z., Shi, X., Liu, X., Wei, M., Huang, A., Zhang, Y., and Liu, X.: The Beijing Climate Center Climate System Model (BCC-CSM): the main progress from CMIP5 to CMIP6, Geoscientific Model Development, 12, 1573–1600, https://doi.org/10.5194/gmd-12-1573-2019, publisher: Copernicus GmbH, 2019.

Yang, M., Blomquist, B., Fairall, C., Archer, S., and Huebert, B.: Air-sea exchange of dimethylsulfide in the Southern Ocean: Measurements from SO GasEx compared to temperate and tropical regions, Journal of Geophysical Research: Oceans, 116, publisher: Wiley Online Library, 2011.

Yoder, J. A. and Kennelly, M. A.: Seasonal and ENSO variability in global ocean phytoplankton chlorophyll derived from 4 years of SeaWiFS measurements, Global Biogeochemical Cycles, 17, publisher: Wiley Online Library, 2003.

Yool, A., Popova, E. E., and Anderson, T. R.: MEDUSA-2.0: an intermediate complexity biogeochemical model of the marine carbon cycle for climate change and ocean acidification studies, Geoscientific Model Development, 6, 1767–1811, https://doi.org/10.5194/gmd-6-1767-2013, 2013.

Yool, A., Palmiéri, J., Jones, C., Sellar, A., de Mora, L., Kuhlbrodt, T., Popova, E., Mulcahy, J., Wiltshire, A., and Rumbold, S.: Spin-up of UK Earth System Model 1 (UKESM1) for CMIP6, Journal of Advances in Modeling Earth Systems, 12, e2019MS001 933, 2020.

Yool, A., Palmiéri, J., Jones, C. G., de Mora, L., Kuhlbrodt, T., Popova, E. E., Nurser, A., Hirschi, J., Blaker, A. T., and Coward, A. C.: Evaluating the physical and biogeochemical state of the global ocean component of UKESM1 in CMIP6 historical simulations, Geoscientific Model Development, 14, 3437–3472, 2021.

Zavarsky, A., Goddijn-Murphy, L., Steinhoff, T., and Marandino, C. A.: Bubble-mediated gas transfer and gas transfer suppression of DMS and CO2, Journal of Geophysical Research: Atmospheres, 123, 6624–6647, publisher: Wiley Online Library, 2018.

Zeng, C., Xu, H., and Fischer, A. M.: Chlorophyll-a estimation around the Antarctica peninsula using satellite algorithms: hints from field water leaving reflectance, Sensors, 16, 2075, publisher: MDPI, 2016.

Zhang, M., Park, K.-T., Yan, J., Park, K., Wu, Y., Jang, E., Gao, W., Tan, G., Wang, J., and Chen, L.: Atmospheric dimethyl sulfide and its significant influence on the sea-to-air flux calculation over the Southern Ocean, Progress in Oceanography, 186, 102 392, publisher: Elsevier, 2020.